

Improving Compound Activity Classification via Deep Transfer and Representation Learning

Vishal Dey,[†] Raghu Machiraju,^{†,‡,¶} and Xia Ning^{*,†,‡,¶}

[†]*Department of Computer Science and Engineering, The Ohio State University, Columbus, OH*

[‡]*Biomedical Informatics, The Ohio State University, Columbus, OH*

[¶]*Translational Data Analytics Institute, The Ohio State University, Columbus, OH*

E-mail: ning.104@osu.edu

Abstract

Recent advances in molecular machine learning, especially deep neural networks such as Graph Neural Networks (GNNs) for predicting structure activity relationships (SAR) have shown tremendous potential in computer-aided drug discovery. However, the applicability of such deep neural networks are limited by the requirement of large amounts of training data. In order to cope with limited training data for a target task, transfer learning for SAR modeling has been recently adopted to leverage information from data of related tasks. In this work, in contrast to the popular parameter-based transfer learning such as pretraining, we develop novel deep transfer learning methods **TAc** and **TAc-fc** to leverage source domain data and transfer useful information to the target domain. **TAc** learns to generate effective molecular features that can generalize well from one domain to another, and increase the classification performance in the target domain. Additionally, **TAc-fc** extends **TAc** by incorporating novel components to

selectively learn feature-wise and compound-wise transferability. We used the bioassay screening data from PubChem, and identified 120 pairs of bioassays such that the active compounds in each pair are more similar to each other compared to its inactive compounds. Overall, **TAc** achieves the best performance with average **ROC-AUC** of 0.801; it significantly improves **ROC-AUC** of 83% target tasks with average task-wise performance improvement of 7.102%, compared to the best baseline **FCN-dmpna** (DT). Our experiments clearly demonstrate that **TAc** achieves significant improvement over all baselines across a large number of target tasks. Furthermore, although **TAc-fc** achieves slightly worse **ROC-AUC** on average compared to **TAc** (0.798 vs 0.801), **TAc-fc** still achieves the best performance on more tasks in terms of **PR-AUC** and **F1** compared to other methods. In summary, **TAc-fc** is also found to be a strong model with competitive or even better performance than **TAc** on a notable number of target tasks.

1 Introduction

Drug discovery is a time consuming and expensive process¹ – it takes at least 10 years and at least \$1 billion to fully develop a drug.² During the initial stages of this process, promising drug candidates are identified by screening large library of chemical compounds, and are then further investigated for specific properties. In order to speed up this process, computational approaches^{3,4} have been adopted, particularly for identifying potential drug candidates during the initial stages of the drug discovery. Computational approaches explore a much larger space of chemical compounds to predict their physio-chemical properties and/or biological activities towards the target. In this paper, we consider the problem of compound bioactivity classification, where a compound is classified as active or inactive based on whether that compound binds to the protein target. Biological activities of compounds are initially examined in a bioassay by measuring their binding affinities or dissociation constants toward the target. Significant research⁵⁻⁷ have established the relationship between the chemical structures and biological activities of compounds, also known as Structure-Activity relation-

ships (SAR).⁵ Several computational approaches⁸ have been developed to model SAR and to predict compound bioactivities from their 2D/3D structures. However, most popular approaches such as deep neural networks require large amounts of labeled data for effective SAR modeling. Thus, limited availability of bioassay data for specific targets still pose a major challenge in effective SAR modeling.⁹

Over the years, several methods¹⁰⁻¹² aimed to improve SAR predictions for specific targets by leveraging activity information from related targets. These methods consider targets to be related, based on the principles from chemogenomics.¹³⁻¹⁶ *The key principle behind these methods is that similar proteins tend to bind to structurally similar compounds.* In this work, we consider proteins belonging to the same protein family to be similar. Thus, leveraging compound activity information from bioassays corresponding to a set of proteins from the same protein family (e.g., G-coupled protein receptors, kinases, peptidases, etc) collectively might better inform the SAR model than the individual bioassays. In essence, transfer learning can enable better SAR modeling by leveraging information from such related bioassays. However, existing methods are instance-based transfer learning methods.¹⁷ They select a subset of data from related bioassays, and then augment the training data for the target task with the selected subset. Existing deep transfer learning based methods¹⁸ for SAR modeling are either parameter-based (such as finetuning), or feature-based; out of which parameter-based methods are more popular. However, such methods can lead to overfitting and negative transfer,¹⁷ especially when the targets are not related. In this regard, we believe that feature-based methods are better in that they can learn the similarity/relatedness between the targets in the latent space in a data-driven manner.

Primarily, we develop an instance-based transfer learning method **TAc** that leverages target information from related bioassays, based on the key principle of chemogenomics as mentioned earlier. We further extend **TAc** to a novel feature-based deep transfer learning method **TAc-fc** that quantitatively measures transferability and explicitly learns what to transfer in a fully data-driven manner. To this end, we develop novel components to learn feature-wise

and compound-wise transferability in order to effectively encode the commonalities among compounds of different tasks. In order to represent compounds, we leveraged the popular idea of Directed Message Passing Neural Network (`dmpn`),¹⁹ and add an attention-based pooling mechanism, denoted as `dmpna`. We collected a set of confirmatory bioassays from PubChem²⁰ that have a single protein target, and are tested on chemical substances. We identified 120 bioassay pairs involving 59 protein targets such that the active compounds in each pair are more similar to each other compared to the inactive compounds. We compared our methods `TAc` and `TAc-fc` with several baselines with respect to two aspects: compound representation and transfer mechanisms. Overall, `TAc-dmpna` achieves the best performance compared to all other methods. Compared to `TAc-dmpna`, `TAc-fc-dmpna` performs slightly worse, but the latter still provides significant performance improvement on some target tasks. This suggests that although the transfer mechanism in `TAc` performs the best overall, the deep transfer mechanism with learned feature-wise and compound-wise transferability can actually benefit some targets. Furthermore, experimental results demonstrate the efficacy of our proposed attention mechanism of `dmpna` in learning better compound features. We provide additional experiments on the compound prioritization problem¹² where `dmpna` clearly outperforms all other compound representation methods.

The rest of the paper is organized as follows. Section 1.1 presents the related works in drug discovery, and transfer learning with applications in SAR predictions. Section 2 presents the materials used for experimental evaluation, experimental results and detailed analyses with discussions. Section 3 presents the conclusions. Section 4 presents the notations and definitions used in this paper, and the proposed methods of transfer learning for activity prediction.

1.1 Related Work

In this section, we provide a brief overview of existing works and divide them across 3 subsections as follows. In section 1.1.1, we summarize notable works on computational

approaches in drug discovery. In section 1.1.2, we provide a brief overview of existing works in transfer learning. In section 1.1.3, we provide an overview of existing methods that uses transfer learning for better SAR modeling.

1.1.1 Computational Methods in Drug Discovery

The first step in the drug discovery process is to conduct bioassays²¹ that screens a large set of compounds for desirable properties (e.g., activity, solubility, toxicity). The findings from these bioassays guide the later steps of the drug discovery process. In order to speed up initial stages of the drug discovery process, computational approaches have been adopted. Computational approaches to predict activities/properties of compounds from their molecular structures have been a significant research area in cheminformatics.^{8,22,23} These approaches rely on the quantitative structure activity/property relationship (QSAR/QSPR)^{5,24} to predict compound activities/properties as expressed in bioassays.

In order to predict such activities/properties, machine learning methods such as classification and regression are typically used. Binary/real-valued observations from bioassay data are used to train these classification/regression methods. Popular conventional classification and regression methods to predict compound activities/properties consist of support vector machines,^{25–28} random forests,^{29,30} Bayesian models,^{31,32} etc. In these methods, compounds are typically represented by hand-crafted molecular fingerprints^{33,34} or descriptors.³⁵ Recently, deep learning methods^{36–40} have demonstrated significant performance improvement over conventional methods across several activity/property prediction tasks.^{41–43} Unlike conventional methods, these methods do not require careful and expensive design of hand-crafted molecular fingerprints or descriptors by domain experts. These methods learn the compound representations from molecular graphs^{19,44–48} and SMILES strings,^{49–51} in a fully data-driven manner for each task. Such learned representations are task-specific and can better encode relevant structures for each task. Thus, such learned representations are often more effective than molecular fingerprints or descriptors. While these deep learning models

have achieved the state-of-the-art performance on several molecular activity/property prediction tasks, these models require large amount of labeled training data to encode relevant patterns into learned representations. Training these models with limited labeled data for certain prediction tasks often leads to sub-par performance.

1.1.2 Transfer Learning

In order to effectively train models with limited labeled data for certain prediction tasks, transfer learning between related tasks has been widely explored in Computer Vision(CV) and Natural Language Processing (NLP).^{52,53} Transfer learning¹⁷ is an emerging research area in which knowledge gained from auxiliary tasks is transferred to improve the predictive performance of the target task. Instead of training a model for the target task from scratch, a popular transfer learning technique, called finetuning,⁵⁴ finetunes the model pretrained from other related tasks. Pretraining does not explicitly learn what/when to transfer and rather relies on the model parameters to encode and transfer information across different tasks. Although pretraining is the most popular transfer learning method, it does not guarantee improvement (due to ‘negative transfer’⁵⁵). Moreover, finetuning a highly parameterized model with limited data may lead to overfitting to the training data and thus, the finetuned model might not generalize well to the test data. Apart from pretraining, another area of deep transfer learning, called domain adaptation has gained a lot of attention.⁵⁶⁻⁵⁸ Domain adaptation methods reduces the effect of the domain shift by learning domain-invariant representations that can generalize well across different tasks. In order to learn such representations, domain adaptation methods either minimize statistical measures⁵⁹⁻⁶¹ of domain shift or use adversarial training.⁶² Following the success of adversarial training in Generative Adversarial Networks (GANs),⁶³ adversarial domain adaptation methods⁶⁴⁻⁶⁶ gained more attention and demonstrated state-of-the-art performances over benchmark CV and NLP datasets. Adversarial domain adaptation methods use adversarial training to learn domain-invariant representations via a mini-max optimization using a feature extractor, a

domain classifier and a label predictor. The principle of adversarial training is used to train the feature extractor to learn domain-invariant representations which are indistinguishable by the domain classifier. Seminal methods in adversarial domain adaptation^{64,65,67} differ in the design choices such as adversarial loss functions, optimization, coupling of weights etc. Other existing methods focus on conditional feature alignment,^{68,69} multi-source transfer,^{70,71} etc. However, these methods have been specifically developed for image domain adaptation or image translation problems. To the best of our knowledge, none of these methods have been widely adapted for graph-structured data. In this work, following the idea of adversarial domain adaptation, we proposed a novel transfer learning method that learns effective compound representations from graph-structured data and transfers relevant information from a related task to the target task.

1.1.3 Transfer Learning in SAR predictions

To alleviate the limited data problem in cheminformatics, various transfer learning^{18,72-75} and multitask learning methods⁷⁶⁻⁸⁰ have been recently developed. Inspired by the success of pretraining followed by finetuning in CV and NLP, Goh et al.⁸¹ proposed ChemNet, where a deep neural network is pretrained on a large set of compounds in a self-supervised manner and then fine-tuned on individual activity/prediction tasks. Following the same idea, Li and Fourches⁸² proposed MolPMoFit which trains a Long Short Term Memory (LSTM)⁸³ on SMILES strings of compounds and then fine-tunes the pretrained model on specific tasks. Although pretraining has been widely studied, existing work in cheminformatics do not demonstrate significant performance improvement over the state-of-the-art supervised models in a single-task setting. Moreover, models trained on SMILES strings do not explicitly leverage the topological information of compounds. However, our methods use molecular graphs as inputs, and hence explicitly leverage the topological information.

Adversarial transfer learning has been rarely explored for SAR predictions and on graph-structured data. To the best of our knowledge, only recently Abbasi et al.⁸⁴ combined

multitask networks and adversarial domain adaptation to learn transferable molecular representations from multiple source bioassays to improve the prediction performance on the target bioassay. The authors evaluated their model on biophysics and physiology data sets such as Tox21, SIDER, BACE, ToxCast and HIV. Experimental results demonstrated that the proposed method outperforms no-transfer methods only on a few target tasks. Moreover, experimental results do not clearly demonstrate the contribution of the adversarial domain adaptation component to the overall performance. Overall, prior work on transfer-learning based SAR modeling do not clearly suggest a performance gain over conventional SAR models over a wide-array of target tasks.

2 Results and Discussion

In this section, we present the materials used for experimental evaluation (Section 2.1), followed by detailed experimental results and discussions (Section 2.2-2.7).

2.1 Materials

In this section, we describe the dataset generation, baseline methods and experimental protocols in detail.

2.1.1 Dataset Generation

We used the real screening data from PubChem to test our methods. PubChem^{20,85} is one of the largest public chemical database with more than 271M substances, 111M unique chemical structures and 293M bioassay data. We selected a set of bioassays from PubChem bioassays [accessed on 2020-12-25] such that each bioassay has a sufficiently large number of active and inactive compounds. Then, we generated pairs of bioassays for transfer learning in accordance to the protocols in below sections 2.1.1.1 and 2.1.1.2.

2.1.1.1 Initial Bioassay Selection and Pruning

We first selected a set of 7,284 confirmatory bioassays that have a single protein target, and are tested on chemical substances. These bioassays have 1,279 unique protein targets in total. Among these protein targets, we were able to identify the organism and protein family information for 961 protein targets within 435 protein families using UniProt.⁸⁶ Among the 435 protein families, we further combined them into 278 families (e.g., Peptidase A1, Peptidase C12, and Peptidase C13 families were combined into peptidase family). Among the 278 families, we selected 10 that have the most protein targets belonging to ‘Human’ organisms. These top-10 protein families are 1) G-protein coupled receptor 1 family, 2) peptidase family, 3) protein kinase family, 4) nuclear hormone receptor family, 5) protein-tyrosine phosphatase family, 6) ABC transporter family, 7) Cytochrome P450 family, 8) Bcl-2 family, 9) G-protein coupled receptor 3 family, and 10) Histone deacetylase family. These protein families involved 269 unique protein targets and covered the major drug targets in drug discovery.^{87,88}

According to the 10 protein families, bioassays with targets from these protein families were then processed as follows:

1. We combined bioassays of a same target into one bioassay, resulting in 269 combined bioassays.
2. For each combined bioassay, we selected its compounds that were tested for inhibition against the target (i.e., the corresponding PubChem activity type specified by the depositor was “inhibitor”).
3. From those inhibitive compounds, we selected the compounds that were specified as either “active” or “inactive” against the target, and discarded the compounds that were specified as “inconclusive” or “undetermined”.
4. If the active/inactive compounds appeared multiple times in the bioassay with a same activity label, we retained one of their records. If the active/inactive compounds

appeared multiple times in the bioassay with different activity labels, we removed the compounds from the bioassays (in our data set, about only 2.08% of compounds for each bioassay on average appear multiple times with different activity levels). We use canonical SMILES strings to detect identical compounds.

After the above processing, each combined bioassay has on average 17,005 unique compounds in total, with 188 active and 16,817 inactive. Furthermore, out of the 269 combined bioassays, 95 bioassays have more than 50 active compounds. Among the 10 protein families involved in the 95 bioassays, 2 protein families had only 1 target with more than 50 active compounds. Thus, we removed these 2 protein families and only used the remaining 8 protein families and their 93 bioassays. This set of 93 bioassays has on average 40,115 compounds, with 521 active and 39,595 inactive. This set of bioassays will be used to create bioassay pairs as will be described in the next section. Table S1 in the Supplementary Materials presents the statistics of each of the 93 bioassays.

2.1.1.2 Transferable Bioassay Pairing

From the 93 processed bioassays, we constructed 765 bioassay pairs such that in each pair, the protein targets of the two bioassays are from the same protein family. We selected targets from a same protein family because based on the key intuition of chemical genomics,^{15,16} proteins from a same family tend to have similar binding pockets and bind to similar compounds – this is the physicochemical foundation to enable possible information transfer across protein targets, and such targets and their bioassays can be used to test transfer learning. We first ensured that each of the 765 pairs of bioassays had balanced active and inactive compounds as follows:

1. In each pair of bioassays, we removed the compounds that appeared in both bioassays but with different activity labels (on average, 2.09% of all unique compounds in a pair of bioassays). This is to avoid any conflicting information across bioassays, which could adversely affect our transfer learning method.

2. For compounds with same activity labels in both the bioassays (on average, 1.82% of all unique compounds in a pair of bioassays), we randomly sampled half of them into one of the bioassays, and the other half into the other. This is to avoid duplication of compounds across bioassays, which could lead to overestimation of predictive performance.
3. After the above steps, for each bioassay of a pair, we used all its active compounds, and randomly sampled the same number of its inactive compounds. If the inactive compounds were not sufficient, we randomly sampled compounds from PubChem that were not active in the bioassay as additional inactive compounds for the bioassays. This is to ensure that each bioassay in a pair has equal number of active and inactive compounds, and thus the learning will not be dominated by either active or inactive compounds. Please note that a bioassay involved in two pairs may have different numbers of active and inactive compounds due to its paired, the other bioassay.

After the above steps, we selected the bioassay pairs such that each bioassay in each pair had at least 50 active compounds retained. There were 635 such pairs and involved 92 bioassays in total. Among the 635 pairs of bioassays, we further selected the pairs as follows such that the active compounds in each pair are similar to each other compared to its inactive compounds:

1. For a pair of bioassay B_i and B_j , and their respective active and inactive compounds, denoted as $\mathcal{X}_{B_i}^+$, $\mathcal{X}_{B_i}^-$, $\mathcal{X}_{B_j}^+$ and $\mathcal{X}_{B_j}^-$, respectively, we calculated the following two types of average compound similarities using Tanimoto coefficient⁸⁹ over Morgan-count fingerprints (with radius 3 and dimension = 2,048): 1) among compounds of same labels across the two bioassays: $\text{sim}(\mathcal{X}_{B_i}^+, \mathcal{X}_{B_j}^+)$, and $\text{sim}(\mathcal{X}_{B_i}^-, \mathcal{X}_{B_j}^-)$; and 2) among compounds of different labels across the two bioassays: $\text{sim}(\mathcal{X}_{B_i}^+, \mathcal{X}_{B_j}^-)$, and $\text{sim}(\mathcal{X}_{B_i}^-, \mathcal{X}_{B_j}^+)$.
2. Based on the similarities, we selected a set of bioassay pairs, denoted as \mathcal{P}_0 , such that

in each pair, the active compounds of the two bioassays are more similar, that is,

$$\mathcal{P}_0 = \{(B_i, B_j) | \text{sim}(\mathcal{X}_{B_i}^+, \mathcal{X}_{B_j}^+) > \text{sim}(\mathcal{X}_{B_i}^+, \mathcal{X}_{B_j}^-) \text{ and } \text{sim}(\mathcal{X}_{B_i}^+, \mathcal{X}_{B_j}^+) > \text{sim}(\mathcal{X}_{B_i}^-, \mathcal{X}_{B_j}^+)\}$$

We identified 329 such pairs. From \mathcal{P}_0 , we further selected a set of bioassay pairs, denoted as \mathcal{P} , such that in each pair, the active compounds in the two bioassays have a similarity above a certain threshold, that is,

$$\mathcal{P} = \{(B_i, B_j) | (B_i, B_j) \in \mathcal{P}_0, \\ \text{sim}(\mathcal{X}_{B_i}^+, \mathcal{X}_{B_j}^+) - \text{sim}(\mathcal{X}_{B_i}^+, \mathcal{X}_{B_j}^-) + \text{sim}(\mathcal{X}_{B_i}^+, \mathcal{X}_{B_j}^+) - \text{sim}(\mathcal{X}_{B_i}^-, \mathcal{X}_{B_j}^+) \geq 0.026\},$$

where 0.026 is the average value of $\text{sim}(\mathcal{X}_{B_i}^+, \mathcal{X}_{B_j}^+) - \text{sim}(\mathcal{X}_{B_i}^+, \mathcal{X}_{B_j}^-) + \text{sim}(\mathcal{X}_{B_i}^+, \mathcal{X}_{B_j}^+) - \text{sim}(\mathcal{X}_{B_i}^-, \mathcal{X}_{B_j}^+)$ among all the pairs.

After the above process, we identified 120 pairs of bioassays in \mathcal{P} , involving 59 bioassays and 7 protein families, with 278 active and 278 inactive compounds in each bioassay on average. Table S2 presents all the pairs and their compound statistics.

2.1.2 Baseline Methods

We tested our TAc and TAc-fc methods with respect to two aspects: 1) compound representations, and 2) transfer mechanisms. Compound representation is key to revealing information among compounds that can be leveraged to transfer across. Transfer mechanisms are critical to enable effective transfer of revealed information across bioassays.

2.1.2.1 Compound Representation Methods

Specifically, we compared our compound representation method `dmpna` (i.e., the feature learner in Section 4.2.2) with the following compound representation methods:

- Binary Morgan fingerprint (`morgan`):³³ `morgan` uses a binary feature vector to present a compound, in which each dimension of the feature vector corresponds to a pre-defined

substructure, and the binary value in that dimension represents if the compound has that substructure or not.

- Morgan count fingerprints (**morgan-c**):³³ **morgan-c** is very similar to **morgan** except that the values in **morgan-c** represent how many corresponding substructures the compound has.
- Directed Message Passing Network (**dmpn**):¹⁹ The **dmpn** method learns molecular structures by passing messages along directed edges over molecular graphs. It produces two representations for each bond through message passing through the two directions along the bond. Then it learns atom representations from the incoming bond representations and generates a compound representation using mean pooling over the atom representations. The **dmpn**¹ method is the state-of-the-art compound embedding learning approach for compound property prediction.

We generated **morgan** and **morgan-c** (with radius = 3 and size = 2,048) using RDKit.⁹⁰ In order to only compare the different compound representation methods, not the transfer learning mechanisms, we used a 2-layer fully-connected network as the classifier **S** over the above baseline feature representations to predict activity labels. We used cross-entropy as the loss function for these baseline methods. The corresponding methods are denoted as FCN-**morgan**, FCN-**morganc** and FCN-**dmpn**, respectively. Note that these three baseline methods do not have information transfer mechanisms – they are single-task compound prediction methods.

2.1.2.2 Learning Methods for Compound Prediction:

We compared TAc and TAc-fc with a transfer learning baseline known as domain-adversarial neural network, denoted as DANN.⁶⁴ We selected DANN because, to the best of our knowledge, there are no existing transfer learning methods over graph-structured data; and DANN is a standard transfer learning baseline method used on other data (e.g., images).⁵⁸ In particular,

¹<https://github.com/chemprop/chemprop> [accessed 2021-01-22]

we adapted DANN to learn compound features from graph-structured data via GNN (e.g., `dmpn` or `dmpna`).

DANN consists of three components: 1) a feature extractor that represents compounds via feature learning; 2) a label predictor that predicts activity labels from learned compound features; 3) a domain classifier that discriminates between the source and target compounds during training. DANN learns compound features that can generalize well from one domain to another such that the learned features contain little discriminative domain information, and enable DANN to accurately predict activity labels.

The objective function in DANN consists of two losses: domain classification loss, and label prediction loss. DANN uses a minimax optimization such that the domain classification loss is minimized with respect to the domain classifier, and is maximized with respect to the feature extractor. Specifically, minimizing the domain classification loss will encourage the domain classifier to correctly discriminate between the source and target compounds. On the other hand, maximizing the domain classification loss will encourage the learning of generalizable compound features.

The feature learner and discriminators in `TAc-fc` are learned via a minimax optimization similarly to how the feature extractor and the domain classifier in DANN are learned. However, `TAc-fc` is different from DANN in that `TAc-fc` learns feature-wise transferability and compound-wise transferability, while DANN only learns compound-wise transferability. Furthermore, following Ganin et al.,⁶⁴ DANN is trained on labeled data from the source domain and unlabeled data from the target domain.

2.1.3 Experimental Protocols

2.1.3.1 Experimental Settings

In our experiments, we split each of the bioassays in a pair into 10 folds. For the target bioassay, we used 1 fold for modeling training, 1 fold for validation and 8 folds for testing. We did the above process 10 times, with a different training fold each time, and reported

the average performance over the 10 times. The above 1:1:8 training-validation-testing ratio follows a typical setting in transfer learning,⁹¹ where it is assumed that the training data is limited so it is needed to leverage other tasks via transfer. We used this cross validation setting because we did not have a benchmark test set for each bioassay; and 10-fold across validation will reduce variance of the model performance. When we transferred the information from the source bioassay to the target bioassay, we used all the folds of the source bioassay and the training fold of the target bioassay in **TAc** in order to maximize the information content in the source bioassay that could be leveraged.

If the baseline methods do not have an information transfer mechanism (e.g., **FCN-morgan**), we applied an additional setting to simulate information transfer: in addition to the target task $\mathcal{T}^{(T)}$'s own training compounds, we also used all the compounds from the source task $\mathcal{T}^{(S)}$ as training data of $\mathcal{T}^{(T)}$. Thus, $\mathcal{T}^{(S)}$'s compounds will enrich $\mathcal{T}^{(T)}$'s training data and bring (i.e., transfer) information from **Src** directly to **Tgt**. This setting is referred to as data transfer, denoted as **DT**. If we only use $\mathcal{T}^{(T)}$'s compounds for training as in conventional single-task models, this setting is denoted as **noT**.

We trained each model using ADAM⁹² optimizer with an initial learning rate 1e-3. All the models are trained up to 40 epochs. We used grid-search to tune all the hyper-parameters such as the dimension d of the compound embedding **r**, hidden-layer dimension of the attention layer for **dmpna**, hidden-layer dimension in **L** and **G**, and batch size. We used the validation set to determine the optimal number of epochs. During training, we evaluated the performance of each model on the validation set at every epoch and choose the trained model at some epoch k that gives the best performance on the validation set; thus we selected k as the optimal number of epochs. We used ROC-AUC metric for the above performance evaluation. All evaluation metrics are discussed in the following section. All the hyper-parameters are reported in Table S3 for reproducibility purposes.

2.1.3.2 Evaluation Metrics

We used the following evaluation metrics: area under the precision-recall curve (PR-AUC), area under the receiver operating characteristic curve (ROC-AUC), precision, sens, accuracy and F1 score.

- Area under the Precision-Recall curve (PR-AUC): A Precision-Recall curve is generated by (precision, recall) value pairs corresponding to variable thresholds. PR-AUC measures the area under the Precision-Recall curve, and provides an aggregate measure of performance across all possible thresholds.
- Area under the Receiver Operating Characteristics curve (ROC-AUC): A Receiver Operating Characteristic (ROC) curve is generated by true positive rates against false positive rates at various threshold values. ROC-AUC measures the area under the ROC curve.
- precision: it is the ratio of correctly predicted positive instances out of all predicted positive instances (e.g. the ratio of predicted active compounds that are truly active).
- sens: it is the ratio of correctly predicted positive instances out of all ground-truth positive instances (e.g. the ratio of active compounds that are correctly predicted as active).
- accuracy: it is the ratio of correctly predicted (positive and negative) instances out of all instances (e.g. the ratio of compounds that are correctly predicted as active/inactive).
- F1-score: it is the harmonic mean of precision and sens.

If the above metrics have higher values, they indicate better performance.

2.1.4 Data and Software Availability

All the data sets and source code are publicly available at <https://github.com/ninglab/TransferAct>.

2.2 Overall Performance

Table 1: Overall Comparison

method	ROC-AUC	PR-AUC	precision	sens	accuracy	F1
FCN-morgan	0.727±0.124	0.729±0.121	0.648±0.104	<u>0.742±0.131</u>	0.661±0.110	<u>0.683±0.105</u>
FCN-morganc	0.731±0.120	0.730±0.118	0.653±0.102	<u>0.735±0.132</u>	0.664±0.107	<u>0.682±0.105</u>
FCN-dmpn	0.754±0.101	0.733±0.102	0.619±0.116	0.739±0.156	0.656±0.087	0.655±0.126
FCN-dmpna	0.755±0.112	0.729±0.112	0.660±0.119	0.712±0.165	0.665±0.101	0.651±0.136
FCN-dmpn (DT)	0.754±0.104	0.735±0.105	0.687±0.106	0.686±0.213	0.669±0.088	0.655±0.140
FCN-dmpna (DT)	<u>0.763±0.108</u>	<u>0.745±0.109</u>	<u>0.702±0.108</u>	0.671±0.213	<u>0.672±0.092</u>	0.645±0.148
DANN-dmpn	0.733±0.103	0.715±0.103	0.671±0.110	0.647±0.215	0.649±0.084	0.623±0.144
DANN-dmpna	0.734±0.102	0.716±0.104	0.676±0.106	0.653±0.226	0.651±0.085	0.624±0.154
TAc-dmpn	0.798±0.103	0.785±0.108	0.729±0.095	0.729±0.146	0.721±0.093	0.714±0.108
TAc-fc-dmpn	0.798±0.102	0.784±0.107	0.729±0.094	0.731±0.142	0.720±0.091	0.715±0.102
TAc-dmpna	0.801±0.102	0.786±0.107	0.731±0.094	0.729±0.143	0.720±0.090	0.713±0.103
TAc-fc-dmpna	0.798±0.105	0.785±0.109	0.730±0.097	0.728±0.147	0.719±0.095	0.713±0.109

In this table, the columns ROC-AUC, PR-AUC, precision, sens, accuracy and F1-score have the average and standard deviation over all bioassays in each performance metric. The best performance values are **boldfaced**. The second best performance values are underlined.

Table 1 presents overall performance comparison between TAc-dmpn, TAc-fc-dmpn, TAc-dmpna, TAc-fc-dmpna, and the baselines. The columns has the average and standard deviation over all bioassays in respective evaluation metrics achieved by the optimal models. Note that for each bioassay, the optimal model of each method is the model that gives the best ROC-AUC value, and thus the performance of each method in other metrics does not necessarily correspond to the optimal performance in those metrics.

Table 1 shows that, overall, TAc-dmpna achieves the best performance compared to all other methods. Specifically, TAc-dmpna achieves the best average ROC-AUC, PR-AUC and precision scores of 0.801, 0.786 and 0.731, respectively. This demonstrates that TAc-dmpna can learn effective compound features for the target task by leveraging source bioassay data,

and correctly predict the compounds of the target bioassay. Furthermore, all variants of TAc and TAc-fc, especially TAc-dmpn, TAc-fc-dmpn, and TAc-fc-dmpna achieve similar performance on average across all metrics. The performance of these three methods are not significantly different in most metrics. This suggests that learning feature-wise and compound-wise transferability via TAc-fc methods does not necessarily provide performance boost on average. However, compared to the best method TAc-dmpna, TAc-fc-dmpn and TAc-fc-dmpna improve ROC-AUC scores of 62% and 39% target tasks, respectively. On the whole, all variants of TAc and TAc-fc significantly outperform all baselines. Specifically, TAc-dmpna improves the average ROC-AUC by 4.9-10.1%, and significantly improves ROC-AUC of at least 83% of target tasks compared to any baseline method. Each of the other variants such as TAc-dmpn, TAc-fc-dmpn and TAc-fc-dmpna improves ROC-AUC of at least 79% of the target tasks compared to any baseline method. This indicates that these methods can effectively transfer relevant information from the source task to the target task. In particular, the transfer learning mechanism in all variants of TAc and TAc-fc can better leverage source domain data than the transfer learning mechanism in other baselines. This is because both TAc and TAc-fc variants can better control the transferable information by incorporating varying degrees of task-relatedness between the source and target tasks during training. Additionally, TAc-fc variants can better extract relevant information from source domain data by learning feature-wise (Section 4.2.5.1) and compound-wise transferability (Section 4.2.5.2).

The best performance among the baseline methods is achieved by FCN-dmpna (DT). Table 2 presents the performance comparison between TAc-dmpna and FCN-dmpna (DT). The **diff%** values in Table 2 are calculated as the percentage difference of average performance in each metric from TAc-dmpna over FCN-dmpna (DT), where the average performance in each metric is calculated as the performance in that metric averaged over all the bioassays. The **t-diff%** values are calculated as the average of task-wise performance improvement (in %) from TAc-dmpna over FCN-dmpna (DT). The **N-impv** values denote the number of improved target tasks where TAc-dmpna performs better than FCN-dmpna (DT) in respective metrics.

Table 2: Performance Comparison of TAc-dmpna vs FCN-dmpna

method	ROC-AUC	PR-AUC	precision	sens	accuracy	F1
TAc-dmpna	0.801	0.786	0.731	0.729	0.720	0.713
FCN-dmpna (DT)	0.763	0.745	0.702	0.671	0.672	0.645
diff%	4.980	5.503	4.131	8.644	7.143	10.543
t-diff%	5.702	6.085	4.876	25.281	7.727	18.464
	(2.80e-19)	(8.00e-21)	(1.69e-11)	(1.73e-09)	(1.19e-29)	(8.93e-20)
N-impv	199 (83%)	192 (80%)	157 (65%)	153 (64%)	201 (84%)	198 (82%)
t-impv%	7.102	8.044	9.293	44.261	9.509	23.532
	(5.56e-22)	(5.51e-26)	(2.81e-27)	(7.36e-25)	(5.02e-35)	(3.60e-26)

In this table, the first two rows has the performance from respective methods averaged over all bioassays in each performance metric. The row `diff%` has the percentage difference of average performance in each metric from TAc-dmpna over FCN-dmpna (DT). The row `t-diff%` has the average of task-wise percentage improvement from TAc-dmpna over FCN-dmpna (DT) in respective metrics, with corresponding p-value in parentheses below. The row `N-impv` has the number and percentage of target tasks where TAc-dmpna performs better than FCN-dmpna (DT) in respective metrics. The row `t-impv%` has the average of task-wise percentage improvement only among the corresponding improved tasks, with corresponding p-values in parentheses below.

Considering only these `N-impv` improved tasks, the average of task-wise performance improvement (in %) are listed as `t-impv%` values. Similar to `t-diff%`, the numbers presented in parentheses in this row are the corresponding p-values for `t-impv%`. A p-value less than 0.05 was considered to be statistically significant.

Clearly, compared to the best baseline method FCN-dmpna (DT), TAc-dmpna improves average ROC-AUC, PR-AUC, precision, sens, accuracy and F1 scores by 4.980%, 5.503%, 4.131%, 8.644%, 7.143%, and 10.543%, respectively. Furthermore, the average task-wise performance difference (i.e., `t-diff%`) from TAc-dmpna over FCN-dmpna (DT) across each metric is 5.702%, 6.085%, 4.876%, 25.281%, 7.727%, and 18.464%, respectively; and these differences are positive and statistically significant (as indicated by their corresponding p-values in parentheses) – hence suggesting that TAc-dmpna significantly improves the task-wise performance over FCN-dmpna (DT). In particular, TAc-dmpna significantly improves the ROC-AUC performance of 199 out of 240 (83%) target tasks with an average task-wise improvement (i.e. `t-impv%`) of 7.102% (p-value: 5.56e-22). Such consistent and significant improvement (demonstrated by `t-impv%` and their corresponding p-values) across all evaluation metrics on a large per-

centage of target tasks (demonstrated by N-impv) provides strong evidence that TAc-dmpna clearly outperforms FCN-dmpna (DT) on majority of target tasks. This further implies that the transfer mechanism in TAc-dmpna is more effective than that in FCN-dmpna (DT). While FCN-dmpna (DT) pays equal attention to both the source and target tasks during training, TAc-dmpna can differentially focus on the two tasks by varying the weightage on the source classification loss (i.e., the trade-off parameter α in equation 3). Note that TAc-dmpna with $\alpha = 1$ is methodologically equivalent to FCN-dmpna (DT). By varying α , TAc-dmpna can incorporate different degrees of task relatedness between the source and target tasks during training. If the two tasks are not that related, a lower α will encourage the learning to focus more on the target task. In essence, learned compound features are more specific to the target task. On the other hand, α as high as 1 will enforce learning of compound features that generalize well across the two tasks. Such features may encode little target task-specific information, and hence, are not effective.

Furthermore, our experimental results in Table 1 demonstrate the efficacy of our proposed attention mechanism of dmpna in learning better compound features. Overall, both dmpna-based methods (i.e., FCN-dmpna and FCN-dmpna (DT)) outperform dmpn-based methods (i.e., FCN-dmpn and FCN-dmpn (DT)). Particularly, compared to FCN-dmpn (DT), FCN-dmpna (DT) improves about half of the target tasks improves ROC-AUC of 152 out of 240 (63%) target tasks and gives significant performance improvement of 3.443% (p-value: 2.64e-18) on those improved target tasks. This demonstrates that the proposed attention mechanism in dmpna enables more effective compound features since it can differentially score atoms based on their relevance towards the final task. However, FCN-dmpna either achieves similar or slightly worse performance compared to FCN-dmpn. This is because dmpna- with slightly more parameters than dmpn- may struggle to capture relevant patterns during training, and thus FCN-dmpna can easily overfit to limited training data of the target task. In essence, this can lead to poor generalization performance on the test data. On the other hand, FCN-dmpna (DT) can generalize well since it is trained on the labeled source data along with the limited target

data. Overall, the attention mechanism can better learn and effectively score the atoms in FCN-dmpna (DT) but not in FCN-dmpna – thereby achieving significant improvement in the former over FCN-dmpn (DT), and marginal improvement in the latter over FCN-dmpn. We will further demonstrate the efficacy of our proposed dmpna in the compound prioritization problem detailed in Section 2.7.

Furthermore, all GNN-based baselines (i.e., FCN-dmpn, FCN-dmpna, FCN-dmpn (DT) and FCN-dmpna (DT)) significantly outperform DANN-based methods. Our experimental results show that both DANN-based methods yield poor or similar performance compared to all other baseline methods. Specifically, the best DANN method (i.e. DANN-dmpna) reduces the average performance by 3-4% over the best baseline method FCN-dmpna (DT) across all evaluation metrics. Such poor performance may be due to the ineffectiveness of domain-invariant compound features to encode necessary task-specific information.

Surprisingly, DANN even performs worse than the fingerprint-based methods (i.e. FCN-morgan and FCN-morganc). As a matter of fact, overall, fingerprint-based methods performs relatively well compared to all other baselines. Compared to GNN-based methods, fingerprint-based methods achieve competitive or even better performance in most evaluation metrics. This could be due to potential overfitting of GNN-based methods in low-data settings. It is known that GNNs require large amounts of training data to extract relevant molecular substructures and to effectively encode meaningful task-specific information. In contrast, fingerprint-based methods are not data-hungry owing to fewer learnable parameters and thus, these methods can perform reasonably well in low-data setting.⁹³

2.3 Top-N Task-wise Performance Comparison

Table 3 presents a fine-grained performance comparison of top-performing methods over all 240 target tasks across different evaluation metrics. The columns corresponding to each evaluation metric has the percentage of tasks for which each method is among the top- k ($k = 1, 3, 5$) best methods with respect to the metric. Note that for each method, we consider

Table 3: Top- N Performance Comparison (%)

method	ROC-AUC			PR-AUC			F1		
	1	3	5	1	3	5	1	3	5
top- N									
FCN-morgan	10	15	20	13	21	30	11	19	23
FCN-morganc	2	13	18	3	17	22	4	17	22
FCN-dmpn	5	9	17	6	11	17	10	19	30
FCN-dmpna	4	10	26	2	7	20	5	11	26
FCN-dmpn (DT)	2	11	23	4	13	24	5	13	22
FCN-dmpna (DT)	5	18	33	6	14	31	2	8	23
DANN-dmpn	2	9	16	1	5	15	3	10	19
DANN-dmpna	2	8	17	1	8	15	2	11	19
TAc-dmpn	18	52	85	17	48	81	12	49	81
TAc-fc-dmpn	12	45	79	15	48	80	17	50	80
TAc-dmpna	22	62	89	14	55	83	13	43	78
TAc-fc-dmpna	16	51	81	20	56	86	15	50	81

In this table, the columns ROC-AUC, PR-AUC, and F1 have the percentage of tasks for which each method is ranked within the top-1, top-3 and top-5 best methods in respective metrics. The best performance values are **boldfaced**.

the best performing model that achieves the optimal performance in each evaluation metric. Therefore, for a given method, the models with the optimal performance in each metric do not necessarily have the same set of corresponding hyperparameters.

Table 3 shows that TAc methods achieve the top-1 best performance among more tasks compared to other methods. For example, TAc-dmpna is the best performing method in terms of ROC-AUC for 22% of tasks, that is, more than 2 folds compared to the best baseline method FCN-morgan (10%). TAc-dmpna consistently achieves the top-3 and top-5 best performance in terms of ROC-AUC on significantly more tasks compare to other methods, with even more folds of difference. Similar trends hold for PR-AUC and F1 as the evaluation metrics. This indicates the strong performance of TAc methods.

Among the four TAc variants, TAc-dmpna is the best in terms of ROC-AUC; TAc-fc-dmpna is overall the best in terms of PR-AUC as it achieves top-1, top-3 and top-5 best performance on more tasks compared to other methods; and TAc-fc-dmpn and TAc-fc-dmpna are the best in terms of F1 as they are either better than or similar to other methods. This indicates that,

while different variants may have advantages of optimizing with respect to different evaluation metrics, **TAc-fc** (Figure 7, with the feature-wise and compound-wise discriminators) is actually also a very strong method or even better compared to **TAc**.

2.4 Comparison on Discriminators

Table 4: Comparison on Discriminators (with `dmpna`)

method	ROC-AUC	PR-AUC	precision	sens	accuracy	F1
TAc	0.801	0.786	0.731	0.729	0.720	0.713
TAc-fc	0.798	0.785	0.730	0.728	0.719	0.713
diff%	-0.375	-0.127	-0.137	-0.137	-0.139	0.000
t-diff%	-0.380	-0.119	-0.072	0.116	-0.150	-0.064
	(2.59e-04)	(4.88e-01)	(7.26e-01)	(7.00e-01)	(5.53e-01)	(8.04e-01)
N-impv	93 (39%)	125 (52%)	119 (50%)	111 (46%)	99 (41%)	112 (47%)
t-impv%	0.921	1.373	2.756	7.037	2.230	3.729
	(7.73e-18)	(4.13e-23)	(1.69e-18)	(5.85e-19)	(4.26e-14)	(1.31e-15)
TAc-c	0.801	0.786	0.730	0.734	0.721	0.716
diff%	0.000	0.000	-0.137	0.686	0.139	0.421
t-diff%	0.010	-0.080	-0.130	1.583	0.128	0.516
	(7.78e-01)	(6.72e-01)	(6.32e-01)	(3.03e-01)	(4.01e-01)	(3.90e-01)
N-impv	135 (56%)	119 (50%)	123 (51%)	126 (52%)	128 (53%)	130 (54%)
t-impv%	0.845	1.330	2.763	8.798	1.971	4.165
	(1.13e-23)	(5.03e-24)	(2.67e-17)	(8.22e-18)	(4.75e-21)	(1.75e-15)
TAc-f	0.799	0.785	0.732	0.722	0.721	0.711
diff%	-0.250	-0.127	0.137	-0.960	0.139	-0.281
t-diff%	-0.192	-0.091	0.218	-0.768	0.170	-0.326
	(4.00e-02)	(3.76e-01)	(5.44e-01)	(1.42e-01)	(3.19e-01)	(4.98e-01)
N-impv	100 (42%)	114 (48%)	124 (52%)	117 (49%)	125 (52%)	123 (51%)
t-impv%	1.029	1.597	2.992	6.999	2.037	3.764
	(3.22e-13)	(2.22e-21)	(3.85e-24)	(1.11e-19)	(9.65e-20)	(1.12e-16)

In this table, the first row block has the average performance of **TAc**. Each of the other row blocks has performance comparison of a **TAc-fc** variant with respect to **TAc**. The metric **diff%** represents the difference of average performance of each comparison method with respect to **TAc**; **t-diff%** represents the average of the task-wise improvement, with corresponding *p*-values in the parentheses below; **N-impv** represents the number of improved tasks and its proportion in the parentheses; and **t-impv%** represents the average of the task-wise improvement only among the improved tasks, with corresponding *p*-values in the parentheses below.

Table 4 presents detailed performance comparison between **TAc**, **TAc-fc**, **TAc-c** and **TAc-f**,

all with `dmpna`. We use `dmpna` here because as in Table 3, `TAc-fc-dmpna` shows better performance on average compared to `TAc-fc-dmpn`. `TAc-c` and `TAc-f` are obtained by removing either the feature-wise discriminator `L` (Section 4.2.5.1), or the compound-wise discriminator `G` (Section 4.2.5.2) from `TAc-fc`. Note that for each bioassay, the optimal model of each method is selected based on ROC-AUC. The `diff%` values in each row block are calculated as the difference (in %) of average performance in each metric from the `TAc-fc` variant over `TAc`. The `t-diff%` values in each row block are calculated as the average of task-wise performance improvements (in %) from the corresponding variant over `TAc`. The row `N-impv` in each row block denotes the number of improved target tasks where the variant performs better than `TAc` in respective metrics, and the average of task-wise performance improvement among only the improved tasks is calculated as `t-impv%` (in %).

Compared to `TAc`, `TAc-fc` achieves similar but slightly worse performance overall (i.e., -0.375% in `diff%` on ROC-AUC); on individual tasks, `TAc-fc` has some statistically significant worse performance in terms of ROC-AUC but similar performance as `TAc` on other evaluation metrics. In addition, `TAc-fc` still provides significant task-wise improvement in about 40–50% tasks across all evaluation metrics. Particularly, it improves the ROC-AUC score for 93 out of 240 (39%) tasks significantly by 0.921% on average (`p-value` = 7.73e-18) over `TAc`. This suggests that the learned feature-wise and compound-wise transferability together have the capacity of improving some target tasks. `TAc-c` performs similarly to `TAc` on average (i.e., 0.000 in `diff%` on ROC-AUC; no significant `t-diff%`). However, `TAc-c` improves over more than half of the tasks with statistical significance on all the evaluation metrics. For example, `TAc-c` achieves better ROC-AUC on 135 out of 240 (56%) tasks. This indicates that the global discriminator (Section 4.2.5.2) that differentiate compounds for the source and target tasks could help improve performance for some tasks. `TAc-f` also shows improvement on about half of the tasks (`N-impv`) with significant improvement that is even higher compared to that in `TAc-c`, but with overall performance (`diff%`) still slightly worse than that of `TAc`. The fact that `TAc-fc`, `TAc-c` and `TAc-f` improve about half of the tasks over `TAc` without

discriminators indicates that they are suitable for certain tasks.

We hypothesize that **TAc-c** can effectively focus on similar compounds of source and target bioassays by learning compound-wise transferability via **G**. We validate this hypothesis with an additional analysis on model predictions and pairwise similarities of predicted compounds with source and target compounds. We find and study the active compounds that are correctly classified as active by **TAc-c** but incorrectly classified as inactive by **TAc** and its variants. Table S4 presents the analysis for these active compounds among target tasks which have at least one such active compound. For each of such active compounds in the target task, we calculated the mean pairwise similarities of that compound with its 5 most similar active compounds in the source task and in the target task, respectively.

On average, **TAc-c** correctly classifies 5.4% (i.e., average of values in ‘cor%’ column in Table S4) of active compounds that are incorrectly classified by **TAc** and its variants. These compounds were found to be 12.4% more similar to the active compounds in the source task than to those in the target task. Furthermore, in 47 out of 97 (48%) tasks with at least one active compound only correctly classified by **TAc-c**, the similarity difference is statistically significant ($p\text{-value} < 0.05$). Overall, this analysis demonstrates that **TAc-c** can better learn the commonalities between source and target compounds, and hence can enhance information transfer from the source task to the target task.

2.5 Parameter Study

Figure 1 presents the parameter study in **TAc-dmpna** on α (i.e., the trade-off parameter between the source and target classification losses as in Equation 4). The study was conducted over the tasks for which **TAc-dmpna** outperforms the other methods. The values in each cell in the figure represent the average of the best performance over the tasks with the optimal choice of other hyperparameters.

Figure 1 shows that **TAc-dmpna** has the best average performance in ROC-AUC, PR-AUC, precision, sens, accuracy and F1-score when $\alpha = 0.5, 0.5, 0.1, 0, 0.5$ and 0.1 , respectively.

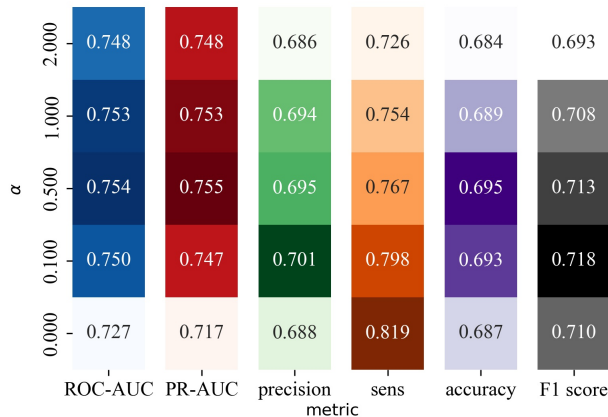


Figure 1: Parameter Study of TAc-dmpna. The columns represent different evaluation metrics. The values in each cell has the average of the best performance achieved with given α and optimal choice of other hyperparameters. Darker cells indicate better performance.

It indicates that weighing the source and target classification losses differently has notable effects on the overall performance. This figure also demonstrates several trends: 1) best average performance is achieved with $\alpha = 0.1$ and 0.5 (i.e., non-zero values) for all the metrics except **sens**; 2) performance degrades especially when α increases. Non-zero values of α as the optimal values indicate that leveraging information from the source task is able to help improve the target task. The fact that the optimal, non-zero α values are relatively small indicates that the training is still more focused on the target tasks, while useful information is transferred from the source tasks. On the other hand, if α is too large (i.e., the source classification loss is given high weightage), the training would be dominated by the source task, and thus the trained model could not well capture the patterns in the target task. That could explain why model performance decreases when α increases.

Figure 2 presents the parameter study in TAc-fc-dmpna in terms of ROC-AUC on α (i.e., the trade-off parameter between source and target losses in Equation 4) and λ (i.e., the trade-off parameter between the classification and discriminator losses in Equation 13). Studies over other metrics are presented in Figure S1 in the Supplementary Materials. The values in each cell of this figure represent the average of the best performance over the tasks where TAc-fc-dmpna outperforms all other methods, with corresponding α and λ , and with optimal

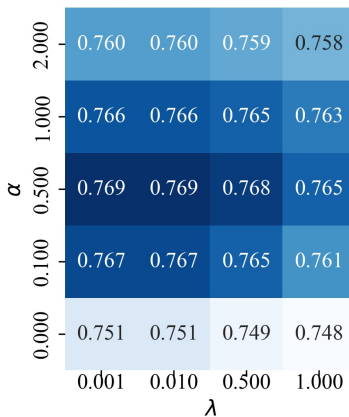


Figure 2: Parameter Study of TAc-fc-dmpna in terms of ROC-AUC

choice of other hyperparameters.

Figure 2 shows that TAc-fc-dmpna has the best performance in ROC-AUC (i.e., 0.769) when $\alpha = 0.5$ and $\lambda = 0.01$ and 0.001, that is, all non-zero values. This demonstrates that a lower weight on the source classification loss than the target classification loss, and a lower weight on discriminator losses (sum of $\mathcal{L}_{(l)}$ and $\mathcal{L}_{(g)}$) will enable effective transfer of relevant information from the source domain. Figure 2 also demonstrates that when α is too small or too large, regardless of what λ is, there is a significant performance drop (as indicated in topmost rows). This effect of α can be explained following the same reasoning presented in the previous section. For the optimal α in each metric, a $\lambda = 0.01$ gives the best performance for most metrics. This implies that TAc-fc-dmpna can effectively leverage source task data to learn transferable compound features (using L) and to selectively focus on similar compounds (using G) during training. Intuitively, for a given α , higher λ values (i.e. higher weight on discriminator losses) will encourage learning of more domain-invariant compound features. Such domain-invariant features contain little task-specific information, and may not be relevant for effective activity classification for the target task, and therefore the overall performance degrades.

2.6 Case Studies: TAc-dmpna

2.6.1 Relation between Performance Improvement and Bioassay Similarity

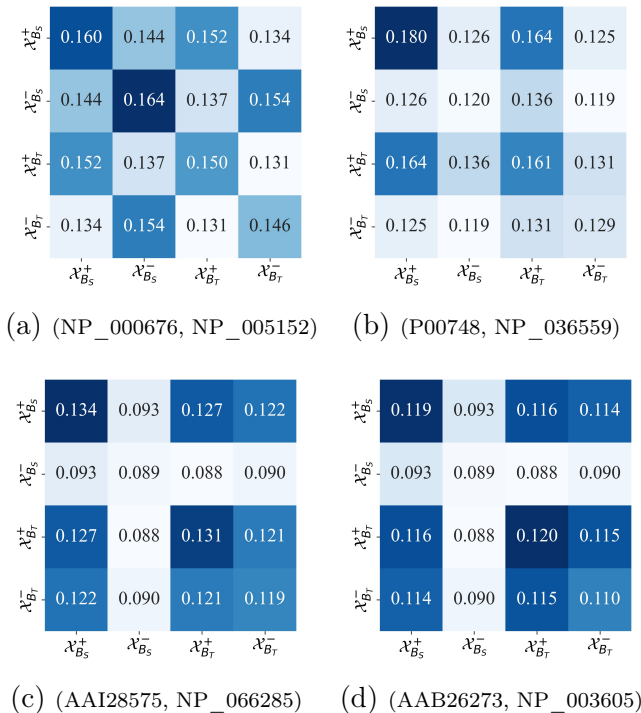


Figure 3: Similarity matrices of target pairs with significant ROC-AUC improvement/degradation

Among 240 tasks, we identified and studied 4 tasks with significant performance difference in ROC-AUC from TAc-dmpna over the best no-transfer baseline method (i.e., FCN-dmpna). Figure 3 presents the average pairwise similarity matrices of the 4 task pairs (captions include the corresponding bioassay PubChem AIDs of the source bioassay and the target bioassay), where Figure 3a and 3b have the target tasks that are significantly improved by TAc-dmpna, and Figure 3c and 3d have the target tasks that are significantly degraded. In the figure, $\mathcal{X}_{B_S}^+$, $\mathcal{X}_{B_S}^-$, $\mathcal{X}_{B_T}^+$ and $\mathcal{X}_{B_T}^-$ denote the active (+) and inactive (-) compounds for the source (B_S) and target (B_T) tasks, and average compound similarities (sim) were calculated using Tanimoto coefficient over Morgan-count fingerprints (with radius=3 and dimension=2,048).

In Figure 3a and 3b, the performance of the target task NP_005152 and NP_036559 was improved from TAc-dmpna over FCN-dmpna by 34.13% and 27.10%, respectively. Figure 3a

and 3b show that for these two target tasks, $\text{sim}(\mathcal{X}_{B_S}^+, \mathcal{X}_{B_T}^+)$ (0.152 in Figure 3a, 0.164 in Figure 3b) is notably greater than both $\text{sim}(\mathcal{X}_{B_S}^+, \mathcal{X}_{B_T}^-)$ (0.134 in Figure 3a, 0.125 in Figure 3b) and $\text{sim}(\mathcal{X}_{B_S}^-, \mathcal{X}_{B_T}^+)$ (0.137 in Figure 3a, 0.136 in Figure 3b). This indicates that if active compounds across bioassays are more similar than compounds with different activity labels across bioassays, TAc-dmpna can better capture the commonalities among those similar active compounds and can better transfer relevant information across bioassays. This transferred information can effectively improve the target task performance. On the other hand, if compounds with different activity labels across bioassays are more similar than compounds with same activity labels, TAc-dmpna can cause transfer of conflicting information. Such a transfer can result in performance degradation for the target task. Such performance degradation in ROC-AUC from TAc-dmpna over FCN-dmpna for the target tasks in pairs (AAI28575, NP_066285) in Figure 3c was 5.74% and (AAB26273, NP_003605) in Figure 3d was 2.34%, respectively. In Figure 3c and 3d, $\text{sim}(\mathcal{X}_{B_S}^+, \mathcal{X}_{B_T}^+)$ and $\text{sim}(\mathcal{X}_{B_S}^+, \mathcal{X}_{B_T}^-)$ values are relatively similar (0.127 vs 0.122 in Figure 3c, 0.116 vs 0.114 in Figure 3d). This indicates that when the similarities between $\mathcal{X}_{B_S}^+$ and $\mathcal{X}_{B_T}^-$ compounds are relatively high, TAc-dmpna could lead to transfer of conflicting information, causing inactive compounds in the target bioassay to be incorrectly classified as active.

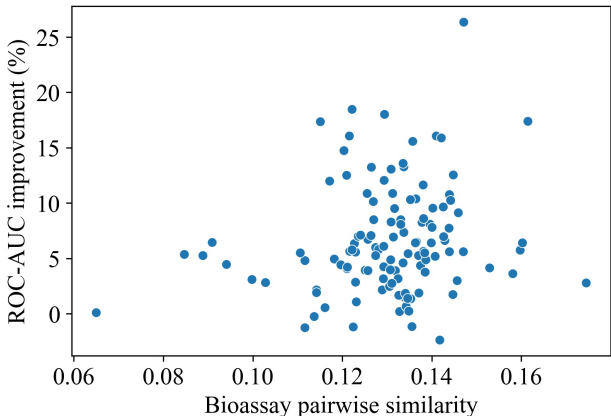


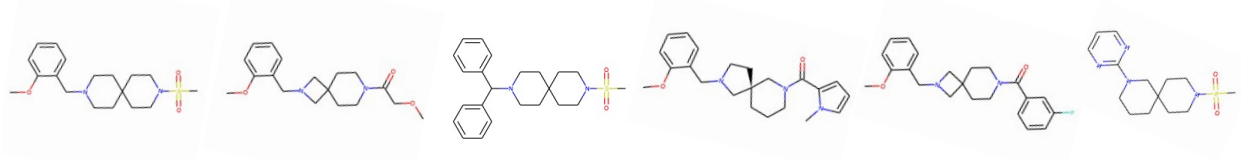
Figure 4: ROC-AUC improvement from TAc over FCN-dmpna vs bioassay similarity

Furthermore, we analyzed the relation between the task-wise ROC-AUC improvement from

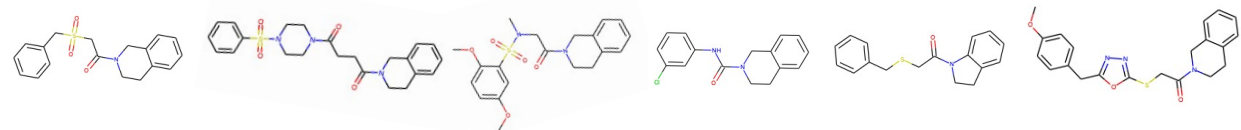
TAc over FCN-dmpna, and the bioassay similarities. Figure 4 presents such relation. Note that the bioassay similarities are calculated as the average of all pairwise compound similarities across two bioassays in the same way as discussed in section 2.1.1.2. Figure 4 demonstrates that there are significant task-wise ROC-AUC improvement (e.g., in the upper right region) when the pairwise similarities are relatively high (e.g., greater than 0.12); and there are marginal improvement (e.g., in the lower left region) when the pairwise similarities are low (e.g., lower than 0.12). This suggests that if bioassay pairs are more similar, TAc can improve the performance over FCN-dmpna by a large margin (e.g., more than 10%). On the other hand, if bioassay pairs are less similar, TAc achieves little or no improvement over FCN-dmpna. Indeed, there are some bioassay pairs that are more similar, yet TAc achieves marginal or negative improvement (e.g., in the lower middle region). This is possibly due to the fact that the performance improvement is not only a function of bioassay similarity; in fact, the improvement can be marginal or negative owing to poor generalization during testing.

2.6.2 Correctly classified compounds possibly due to more similar compounds in the source bioassay

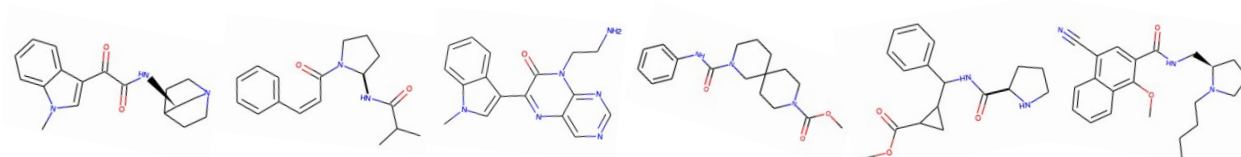
In this section, we identified (i) a few compounds that were correctly classified by TAc but incorrectly classified by the baselines, and (ii) a few compounds incorrectly classified by TAc but correctly classified by the baselines. Figure 5 (a) and (b) present two such examples for (i); and Figure 5 (c) and (d) present two such examples for (ii). In each figure, the left-most compound is the compound to be classified as active/inactive from the target bioassay (referred as $\mathbf{x}^{(T)}$) and the others are the top-5 most similar compounds (referred as $\mathcal{X}_{B_S}^*$) to $\mathbf{x}^{(T)}$ from the corresponding source bioassay. The mean pairwise Tanimoto coefficient between $\mathbf{x}^{(T)}$ and $\mathcal{X}_{B_S}^*$ in Figure 5 (a), (b), (c), and (d) are 0.407, 0.428, 0.210 and 0.143, respectively. Thus, in Figure 5 (a) and (b), $\mathbf{x}^{(T)}$ s are structurally more similar to their corresponding $\mathcal{X}_{B_S}^*$. Relatively, in Figure 5 (c) and (d), $\mathbf{x}^{(T)}$ s are less similar to their corresponding $\mathcal{X}_{B_S}^*$. This suggests that TAc classifies some compounds correctly probably



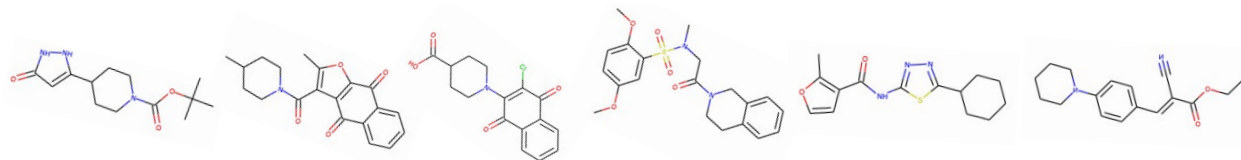
(a) A *correctly* classified compound from the target bioassay NP_000752 and its top-5 most similar compounds from the source bioassay NP_000762



(b) A *correctly* classified compound from the target bioassay NP_660205 and its top-5 most similar compounds from the source bioassay NP_004337



(c) An *incorrectly* classified compound from the target bioassay NP_000752 and its top-5 most similar compounds from the source bioassay NP_000762



(d) An *incorrectly* classified compound from the target bioassay NP_660205 and its top-5 most similar compounds from the source bioassay NP_004337

Figure 5: Visualization of a few selected compounds from the target bioassay and their corresponding top-5 most similar compounds from the source bioassay.

due to the fact that those compounds have very similar compounds in the source bioassay.

2.7 Compound Prioritization using dmpna

We also explored the potential of using **dmpna** for compound prioritization purposes. We develop a comprehensive learning-to-rank method **gnnCP** for effective compound prioritization that jointly learns molecular graph representations via **GNN** and a scoring function using the representations. The learning methods for compound prioritization is described in Section 4 in the Supplementary Materials.

2.7.1 Materials

Baselines: We compare `gnnCP` with the following feature vectors using the same scoring and loss functions: (i) binary Morgan fingerprints (`morgan`), (ii) morgan count fingerprints, (`morgan-c`), (iii) bioassay-specific compound features¹² computed using Tanimoto coefficient on binary Morgan fingerprints (`morgan-ba`), (iv) 200-dimensional RDKit descriptors (`RDKit200`), and (v) directed message passing network¹⁹ (`dmpn`). We generate binary Morgan fingerprints and Morgan-count fingerprints (with radius = 2 and size = 2,048) using RDKit.⁹⁰ Codes for computing the RDKit descriptors are available in the `Descriptastorus` package.⁹⁴

Experimental Protocol: In order to evaluate the overall ranking performance, we perform 5-fold cross validation. We randomly split each bioassay into five folds. In each run, four folds of each bioassay are used for training and the other fold is used for testing. We record optimal values of each performance metric averaged over the five folds. Finally, we report the average of all such recorded optimal values of each performance metric over all the bioassays. For each bioassay, we train the models using Adam⁹² optimizer with an initial learning rate $\in \{5e-3, 1e-3, 5e-4\}$. We use grid-search to tune all the hyperparameters such as the dimension of the graph representation d , hidden dimension of the attention layer and batch size. Specifically, we use $d \in \{25, 50, 100\}$ for `dmpn` and `dmpna`, hidden dimension of the attention layer $\in \{5, 10, 20\}$ for `dmpna`. We use batch size $\in \{128, 256, 512\}$, and $\lambda = 1e-6$ for all the models. All the models are trained for 50 epochs.

Evaluation: We evaluate all the methods using a set of 105 single-target confirmatory bioassays from PubChem.²⁰ These bioassays all use IC_{50} to measure compound binding affinities and have at least 50 active compounds. For each bioassay, we only keep the active compounds, and remove duplicate compounds and those with identical IC_{50} values. We evaluate the ranking performance using concordance index (CI), recall@ k ($R@k$), Normalized

Discounted Cumulative Gain@ k ($\text{ndcg}@k$),¹² where $k = 3, 5, 10$. We also use $\text{R}@k\%$ and $\text{ndcg}@k\%$, where we consider top $k\%$ ($k=5,10$) of the test fold compounds in r .

2.7.2 Results

Table 5: Overall Performance Comparison of `gnnCP`

method	CI	R@3	R@5	ndcg@3	ndcg@5	R@5%	ndcg@5%
<code>morgan</code>	0.706	0.543	0.644	0.814	0.816	0.420	0.838
<code>morgan-c</code>	0.711	0.545	0.655	0.815	0.819	0.437	0.846
<code>morgan-ba</code>	0.687	0.500	0.626	0.789	0.797	0.375	0.816
<code>RDKit200</code>	0.687	0.519	0.632	0.790	0.797	0.396	0.813
<code>dmpn</code>	<u>0.731</u>	<u>0.643</u>	<u>0.709</u>	<u>0.854</u>	<u>0.847</u>	<u>0.579</u>	<u>0.896</u>
<code>dmpna</code>	0.748	0.686	0.740	0.881	0.867	0.686	0.936
<code>diff%</code>	2.353	6.608	4.460	3.114	2.421	18.428	4.475
<code>t-diff%</code>	2.535	7.645	4.720	3.406	2.569	24.578	4.979
<code>p-value</code>	1.14e-10	4.89e-10	9.87e-13	1.42e-12	2.25e-12	3.95e-15	1.83e-11

In this table, the columns have the respective average of each performance metric over all bioassays obtained by the respective optimal hyperparameter settings. The best/second best performance under each metric is **bold**/underlined.

Table 5 presents the performance comparison between `dmpna`, `dmpn` and the baselines. Overall, `dmpna` significantly performs better than all the baselines including `dmpn`, across all performance metrics. The average performance improvement from `dmpna` over `dmpn` in terms of CI, recall@3, recall@5, ndcg@3, ndcg@5, recall@5%, ndcg@5% and is 2.353%, 6.608%, 4.460%, 3.114%, 2.421%, 18.429%, and 4.475%, respectively. Furthermore, compared to `dmpn`, the average bioassay-wise performance improvement from `dmpna` is most significant in terms of recall@3, recall@5, ndcg@3, ndcg@5, recall@5%, and ndcg@5% (p-values: 4.89e-10, 9.87e-13, 1.42e-12, 2.25e-12, 3.95e-15, and 1.83e-11, respectively). This indicates that `dmpna` can rank the top-most compounds better than `dmpn`. Unlike mean pooling in `dmpn`, attention mechanism in `dmpna` can differentially focus on atoms based on the relevance of each atom to the prioritization problem. This demonstrates the ability of `dmpna` to better differentiate compounds and to achieve effective compound prioritization. Furthermore, `dmpna` and `dmpn` significantly outperforms all the fingerprint-based baselines across all performance

metrics. Compared with the best performing fingerprint-based baseline `morgan-c`, in terms of CI, recall@3, recall@5, ndcg@3, ndcg@5, recall@5%, and ndcg@5%, the average performance improvement from `dmpna` is 5.247%, 25.724%, 13.094%, 8.140%, 5.871%, 56.875%, and 10.637%, respectively; and from `dmpn` in terms of CI, recall@3, recall@5, ndcg@3, ndcg@5, recall@5%, and ndcg@5% is 2.827%, 17.932%, 8.266%, 4.874%, 3.369%, 32.464%, and 5.898%, respectively. This demonstrates that the learned representation out of `gnnCP` can effectively encode useful molecular substructure information, and thus, are more effective for compound prioritization.

3 Conclusions

We have developed `TAc` that effectively leverages source bioassay data to improve the performance of the target task. We also proposed a variant of `TAc`, i.e., `TAc-fc` that additionally learns feature-wise and compound-wise transferability. We conducted an exhaustive array of experiments and analyses that suggest that `TAc-dmpna` is the best-performing method on average across all target tasks. The proposed variant is also a very strong method and even better compared to `TAc` on certain target tasks. Furthermore, in ablation studies, we also showed that `TAc-c-dmpna` can even improve performance for more than half of the target tasks compared to `TAc-dmpna`. Our analyses further demonstrated that learning compound-wise transferability via `G` can better encode the commonalities between compounds across bioassays. We also provided a parameter study to demonstrate the effect of α and λ on our proposed methods. Additionally, we demonstrated the efficacy of our proposed `dmpna` in both compound activity and compound prioritization problems since it performed better than any other compound representation methods.

In this work, we paired the bioassays if their corresponding protein targets belong to the same protein family. In other words, when we paired the bioassays, the corresponding pair of tasks are assumed to be related. We assumed that leveraging activity information from

related protein targets (i.e., targets belonging to the same protein family) can improve the target task performance. However, we observed TAc did not improve all the targets compared to the best no-transfer baseline method FCN-dmpna. This suggests occurrence of potential negative transfer. In future works, we will focus on developing a more principled approach to determine task-relatedness. Given a target task, our current method only consider a single source task. This severely limits the scope of transfer from only one related task, and can also impact the performance on the target task if the learning is too focused on the source task. Our future work will incorporate multiple source tasks for each target task by simultaneously learning task-relatedness in a data-driven manner.

4 Computational Methods

4.1 Notations and Definitions

Table 6: Notations

method	meanings
c/B	compound/bioassay
$\mathcal{G} = (\mathcal{A}, \mathcal{E})$	molecular graph with set of atoms \mathcal{A} and bonds \mathcal{E}
u	an atom in \mathcal{G}
(u, v)	a bond connecting atoms u and v in \mathcal{G}
$\mathcal{N}(u)$	neighbors of atom u in \mathcal{G}
\mathcal{X}	set of compounds in a bioassay
\mathcal{Y}	set of labels corresponding to \mathcal{X}
\mathbb{X}	input feature space
\mathbb{Y}	label space
$\mathcal{D} = \{\mathbb{X}, P(\mathcal{X})\}$	a domain consisting of \mathbb{X} and marginal probability distribution $P(\mathcal{X})$
$\mathcal{T} = \{\mathbb{Y}, \omega(\cdot)\}$	a task consisting of label space and a decision function $\omega(\cdot)$
\mathbf{h}	hidden state
\mathbf{r}	molecular representation out of GNN
\mathbf{z}	scaled molecular representation

In this section, we listed the notations and definitions used in this paper. Table 6 presents a list of notations and their meanings. We represent a compound c using a molecular graph \mathcal{G}_c . \mathcal{G}_c is denoted as $\mathcal{G}_c = (\mathcal{A}_c, \mathcal{E}_c)$, where \mathcal{A}_c is the set of atoms, and \mathcal{E}_c is the set of

corresponding bonds in c . We denote the set of compounds in a bioassay B as \mathcal{X}_B , and the activity labels of those compounds accordingly as \mathcal{Y}_B . In this paper, we use a label ‘1’ or ‘0’ to indicate that a compound is active or inactive in a bioassay, respectively.

We use the following definitions related to transfer learning.

- **Domain:** a domain \mathcal{D} is a set of labeled compounds $\mathcal{D} = \{c_i = (\mathbf{x}_i, y_i) | \mathbf{x}_i \in \mathbb{X}, y_i \in \mathbb{Y}, i = 1, \dots, |\mathcal{D}|\}$, where the compounds $\{\mathbf{x}_i\}$ are represented in a feature space \mathbb{X} , and their activity labels $\{y_i\}$ are represented in a label space \mathbb{Y} ; $|\mathcal{D}|$ is the size of the domain (i.e., the number of (\mathbf{x}_i, y_i) pairs). In our transfer learning, we will have two domains: a source domain, denoted as $\mathcal{D}^{(S)}$, and a target domain, denoted as $\mathcal{D}^{(T)}$. In general, these two domains can have different numbers of compounds with different compound feature representations, and also different label sets. We use superscript $^{(S)}$ and $^{(T)}$ to represent information associated with the source domain and the target domain, respectively. For example, $\mathbf{x}^{(T)}$ represents a compound from the target domain. In addition, we use \mathcal{X} to represent the set of compound features $\{\mathbf{x}_i\}$, that is, $\mathcal{X} = \{\mathbf{x}_i | \mathbf{x}_i \in \mathbb{X}\}$, and \mathcal{Y} to represent the set of compound labels, that is, $\mathcal{Y} = \{y_i | y_i \in \mathbb{Y}\}$. Thus, \mathcal{D} can also be represented as $\mathcal{D} = (\mathcal{X}, \mathcal{Y})$.
- **Task:** Given a domain $\mathcal{D} = \{(\mathbf{x}_i, y_i)_{i=1, \dots, |\mathcal{D}|}\}$, a task \mathcal{T} is to learn a model that maps each \mathbf{x}_i to its corresponding y_i . In our transfer learning, we will have two tasks: a source task, denoted as $\mathcal{T}^{(S)}$, and a target task, denoted as $\mathcal{T}^{(T)}$. $\mathcal{T}^{(S)}$ and $\mathcal{T}^{(T)}$ learn from the source domain $\mathcal{D}^{(S)}$ and the target domain $\mathcal{D}^{(T)}$, respectively.
- **Transfer Learning:** Transfer learning learns and transfer information from source task $\mathcal{T}^{(S)}$ to the target task $\mathcal{T}^{(T)}$, and helps improvement the performance of $\mathcal{T}^{(T)}$. The underlying assumptions are 1) the target domain $\mathcal{D}^{(T)}$ does not have sufficient information for $\mathcal{T}^{(T)}$ to learn a good model; and 2) there are commonalities between $\mathcal{D}^{(S)}$ and $\mathcal{D}^{(T)}$ and such commonalities can be transferred from $\mathcal{D}^{(S)}$ to $\mathcal{D}^{(T)}$, and used to improve $\mathcal{T}^{(T)}$.

4.2 Methods

In this section, we present our two transfer learning methods: **TAc** and **TAc-fc**. We first introduce the overall architecture of **TAc** in section 4.2.1, and then discuss each component in detail in subsequent sections (i.e., sections 4.2.2 and 4.2.3). We discuss the end-to-end optimization process in section 4.2.4. We then introduce **TAc-fc** with additional components that learns feature-wise and compound-wise transferability, and finally discuss the optimization process in section 4.2.5.

4.2.1 Overall Architecture of TAc

TAc learns to generate transferable features that can generalize well from one domain to another, and increase the predictive power for classification in the target domain. Figure 6 presents the overall architecture of the proposed **TAc**. **TAc** consists of two components: 1) a feature learner **F**, that learns to represent chemical compounds; and 2) a domain-wise classifier **S**, that classifies chemical compounds of each domain. Below, we discuss each component of **TAc** in detail.

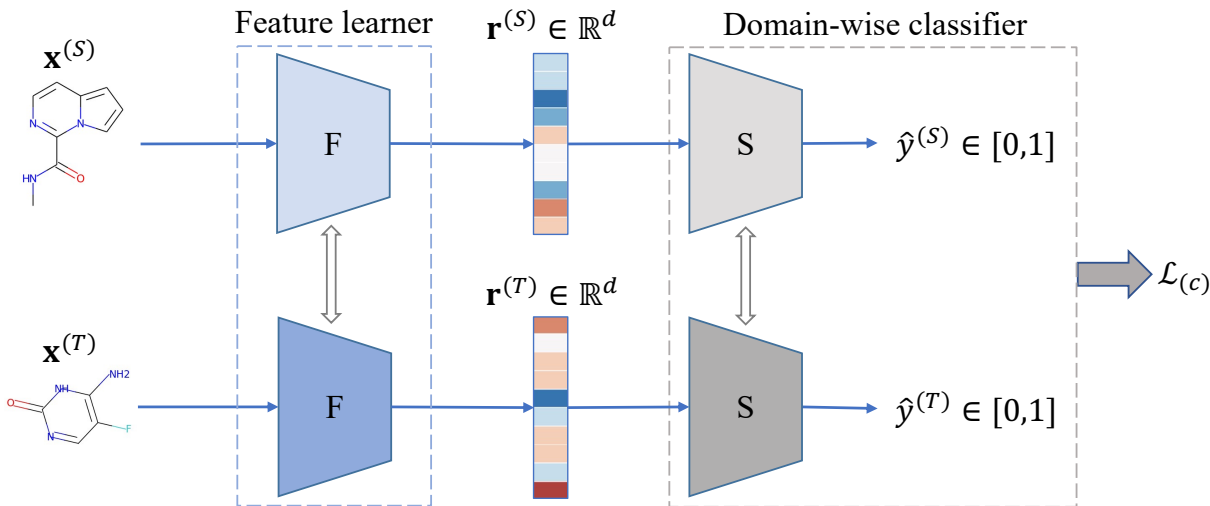


Figure 6: Proposed architecture of **TAc**. The feature learner **F** learns compound representations \mathbf{r} given the corresponding molecular graph. The domain-wise classifier **S** classifies the compound as active/inactive.

4.2.2 Learning Compound Representations

This section describes how the feature representations of compounds are learned. In TAc, the feature representations of chemical compounds are learned in a data-driven fashion. Compared to using static fingerprints or fixed feature representations of molecular structures,³³ such learned features will be more adapted to the learning task and enable optimal performance. We leverage the popular idea of graph neural networks,⁹⁵ and use the Directed Message Passing Neural Network, denoted as **dmpn**, developed in Yang et al.¹⁹ Given a molecular graph $\mathcal{G}_c = (\mathcal{A}_c, \mathcal{E}_c)$ for a compound c , **dmpn** learns a feature vector, also called an embedding, of c using graph convolution, by passing messages along directed edges over molecular graphs. In **dmpn**, two representations for each bond are learned via message passing through the two directions along the bond. Then atom representations are learned from the representations of their incoming bonds. In the end, the compound representation is generated via mean pooling over all the atom representations. Details about **dmpn** are presented in Section 1 in the Supplementary Materials, and also available in Yang et al.¹⁹

Based on **dmpn**, we further improve the compound representation learning by introducing an attention mechanism inspired from Graph Attention Networks⁹⁶. This new method is referred to as **dmpn** with attention, denoted as **dmpna**. Specifically, we replace the mean-pooling in **dmpn** with an attention-based pooling mechanism as follows,

$$\mathbf{r}_c = \sum_{u \in \mathcal{A}_c} (\mathbb{1} + w_u) \odot \mathbf{s}_u, \quad (1)$$

where \odot is the element-wise product, \mathbf{s}_u is the learned representation of atom u as in **dmpn**, w_u is the attention weight on atom u calculated as follows,

$$w_u = \frac{\exp(f_a(\mathbf{s}_u))}{\sum_{v \in \mathcal{A}_c} \exp(f_a(\mathbf{s}_v))} \quad (2)$$

where $f_a(\cdot)$ is a 2-layer feed-forward network with a ReLU activation function after the

hidden layer. That is, the attention learns a specific weight on each atom. Thus, the attention mechanism in `dmpna` can differentially focus on atoms based on the relevance of each atom towards the final predictive task. The network to learn compound embeddings is denoted as \mathbf{F} (i.e., \mathbf{F} is `dmpn` or `dmpna`).

4.2.3 Learning to Classify Compounds of Each Domain

This section describes how the compounds of each domain are classified as active/inactive using the learned feature representations. Given the compound embedding \mathbf{r} , the domain-wise classifier classifies each compound in a given domain as active or inactive with respect to that domain using a two-layer fully-connected neural network \mathbf{S} as follows,

$$\hat{y} = \mathbf{S}(\mathbf{r}), \tag{3}$$

with ReLU at the hidden layer and sigmoid at the output layer. The outputs of \mathbf{S} are the probabilities of input compounds from source/target domain being active in the source/target domain.

To learn \mathbf{S} , the loss function $\mathcal{L}_{(c)}$ for the classifier is defined as follows,

$$\begin{aligned} \mathcal{L}_{(c)}(\Omega, \Phi) = & -\alpha \frac{1}{n^{(S)}} \sum_{\mathbf{x}^{(S)} \in \mathcal{X}^{(S)}} [y^{(S)} \log(\hat{y}^{(S)}) + (1 - y^{(S)}) \log(1 - \hat{y}^{(S)})] \\ & - \frac{1}{n^{(T)}} \sum_{\mathbf{x}^{(T)} \in \mathcal{X}^{(T)}} [y^{(T)} \log(\hat{y}^{(T)}) + (1 - y^{(T)}) \log(1 - \hat{y}^{(T)})], \end{aligned} \tag{4}$$

where $y^{(S)}/y^{(T)}$ is the ground-truth activity label of each compound in domain S/T , $n^{(S)}/n^{(T)}$ is the number of compounds in $\mathcal{X}^{(S)}/\mathcal{X}^{(T)}$ (i.e., $n = |\mathcal{D}|$), α is a hyperparameter to trade-off the two classification losses, and Ω and Φ are learnable parameters of \mathbf{F} and \mathbf{S} , respectively. Please note that both the source domain and target domain use the same classifier \mathbf{S} . Therefore, if the source and target domain have common compounds or very similar compounds, when these compounds have same labels in the two domains, they will induce small clas-

sification errors in the both domains; when these compounds have different labels in the two domains, they will induce large errors in one domain and small errors in the other. By minimizing the loss $\mathcal{L}_{(c)}(\Omega, \Phi)$, it will encourage common or similar compounds that have same labels in the two domains to be more focused on through learning, and prevent the transfer of conflicting information across domains.

4.2.4 TAc Model Optimization

This section presents the optimization process of the proposed TAc. TAc constructs an end-to-end transfer learning framework with the above two components: 1) feature learner \mathbf{F} , and 2) domain-wise classifier \mathbf{S} . We solve for TAc through minimizing the loss function $\mathcal{L}_{(c)}$. In other words, we solve the following optimization problem:

$$\hat{\Omega}, \hat{\Phi} = \arg \min_{\Omega, \Phi} \mathcal{L}_{(c)}(\Omega, \Phi), \tag{5}$$

where Ω and Φ are the learnable parameters of \mathbf{F} and \mathbf{S} , respectively. Minimizing $\mathcal{L}_{(c)}$ will minimize the classification error in each domain while preventing transfer of conflicting information across domains, hence enabling the feature learner \mathbf{F} to learn better compound features for effective classification in each domain. Since the same \mathbf{F} and \mathbf{S} are used for both the source and target tasks, minimizing $\mathcal{L}_{(c)}$ also enables transfer of relevant information through the shared parameters of \mathbf{F} and \mathbf{S} . Intuitively, the amount of transferable information from the source domain to the target domain is determined by the degree of task-relatedness between those domains. In this work, the degree of task-relatedness between the source and target domains is essentially controlled through the hyperparameter α . We will consider learning task-relatedness or α in a data-driven manner in our future works.

4.2.5 Variant of TAc: TAc-fc

In this section, we propose a variant of TAc where we incorporate additional components to selectively learn feature-wise and compound-wise transferability. We denote this variant as TAc-fc. Figure 7 presents the overall architecture of the proposed TAc-fc. In addition to the feature learner F and the label classifier S, TAc-fc consists of two more components: 1) a feature-wise discriminator L, that learns the transferability of each learned feature (Section 4.2.5.1); and 2) a compound-wise discriminator G, that separates chemical compounds into source and target domains (Section 4.2.5.2). We refer to TAc with the feature-wise discriminator only as TAc-f, and TAc with the compound-wise discriminator only as TAc-c. Below, we discuss each component in detail and also the optimization of the proposed method.

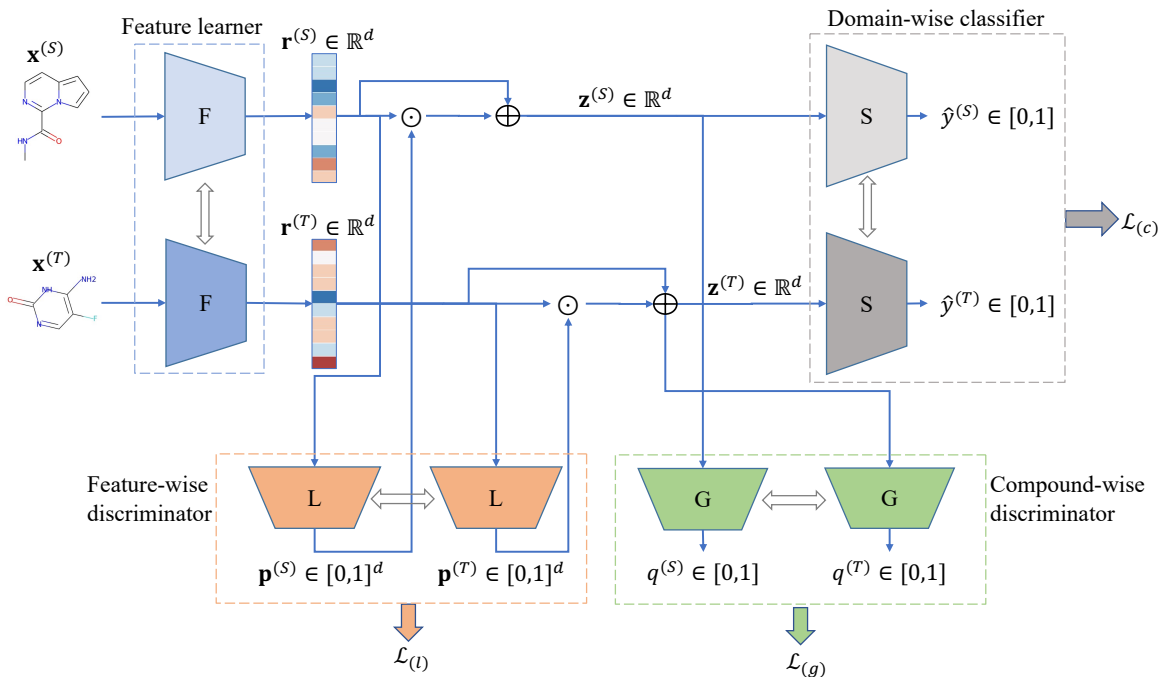


Figure 7: Proposed architecture of TAc-fc. The feature learner F learns compound embedding \mathbf{r} given the corresponding molecular graph. The feature-wise discriminator L learns feature-wise transferability given the learned compound embedding \mathbf{r} . \mathbf{r} is further scaled into \mathbf{z} using its feature entropy from \mathbf{p} out of L. The compound-wise discriminator G learns the compound-wise transferability given \mathbf{z} . The domain-wise classifier S classifies the compound as active/inactive.

4.2.5.1 Learning Transferability of Individual Features

Given the learned compound embedding $\mathbf{r} \in \mathbb{R}^d$ out of \mathbf{F} (discussed in Section 4.2.2), the feature-wise discriminator of TAc-fc learns the transferability of each embedding feature in \mathbf{r} using a two-layer neural network \mathbf{L} as follows,

$$\mathbf{p} = \mathbf{L}(\mathbf{r}), \tag{6}$$

where \mathbf{L} has a hidden layer with ReLU, and an output layer with sigmoid. Note that $\mathbf{p} = [p_1, p_2, \dots, p_d]$ has the same dimension as \mathbf{r} , and $p_i \in [0, 1]$ represents the probability that the i -th embedding feature in \mathbf{r} is specific to the source domain. Thus, the feature-wise discriminator determines whether the input compound features (not the input compounds) belong to the source domain or not. For bioactivity prediction problems, if $\mathcal{D}^{(S)}$ and $\mathcal{D}^{(T)}$ have compounds for protein targets that are from a same protein family, it is very likely that their active compounds are similar and share similar substructures (e.g., pharmacophores). In this case, intuitively, the feature-wise discriminator here could learn and represent such similar substructures.

We further quantify the transferability of each embedding feature using its entropies as follows,

$$H(p_i) = -p_i \log p_i - (1 - p_i) \log(1 - p_i). \tag{7}$$

If p_i is very large or very small and it will have a low entropy, it indicates the i -th embedding feature is very likely or very unlikely to be specific to the source domain, and thus it is less likely to be common across domains; if p_i is close to 0.5 and with a high entropy, the feature is less specific to any of the domains and more likely to be common across domains, and therefore can be used for information transfer across domains.

We then scale compound embedding \mathbf{r} into \mathbf{z} using feature entropies as follows,

$$\mathbf{z} = (\mathbb{1} + \mathbf{H}) \odot \mathbf{r}, \tag{8}$$

where $\mathbf{H} = [H(p_1), H(p_2), \dots, H(p_d)] \in \mathbb{R}^d$, and \odot represents element-wise dot-product. Each feature is scaled with its entropy and added with itself. Intuitively, the self-addition reduces the loss of informative features due to improper scaling. Thus, in \mathbf{z} , domain-invariant embedding features are scaled larger than domain-specific embedding features ($\mathbf{H} \geq 0$). We will use \mathbf{z} as input to the following components.

To learn the feature-wise discriminator, the loss function $\mathcal{L}_{(l)}$ is defined as follows,

$$\begin{aligned} \mathcal{L}_{(l)}(\Omega, \Theta) &= -\frac{1}{n^{(S)}} \sum_{\mathbf{x}^{(S)} \in \mathcal{X}^{(S)}} \frac{1}{d} \sum_{i=1 \dots d} \log(p_i^{(S)}) \\ &\quad - \frac{1}{n^{(T)}} \sum_{\mathbf{x}^{(T)} \in \mathcal{X}^{(T)}} \frac{1}{d} \sum_{i=1 \dots d} \log(1 - p_i^{(T)}), \end{aligned} \tag{9}$$

where $n^{(S)}/n^{(T)}$ is the number of compounds in $\mathcal{X}^{(S)}/\mathcal{X}^{(T)}$ (i.e., $n = |\mathcal{D}|$); Ω and Θ are learnable parameters of \mathbf{F} (compound representation learning network as in Section 4.2.2) and \mathbf{L} (feature-wise discriminator network as in Equation 6), respectively; and d is the dimension of compound feature embeddings. Note that in Equation 9, $p_i^{(S)}$ and $p_i^{(T)}$ both measure an embedding feature’s probability of being specific to the *source domain*; superscripts $^{(S)}/^{(T)}$ here indicate that the compounds, whose features are measured, are from source/target domain, respectively.

To have an accurate feature-wise discriminator, embedding features specific to the source/target domain should have large/small probabilities (i.e., large $p_i^{(S)}$ and small $p_i^{(T)}$) with respect to the source domain, and thus make the $\mathcal{L}_{(l)}$ value small. Therefore, minimizing $\mathcal{L}_{(l)}$ will encourage accurate probabilities. Meanwhile, the feature learner \mathbf{F} should encourage the learning of more transferable embedding features, which will have probabilities close to 0.5 and thus make the $\mathcal{L}_{(l)}$ value large. Therefore, maximizing $\mathcal{L}_{(l)}$ will encourage more transferable embedding features being learned and learned well. To combine these two aspects, an adversarial optimization will be applied to $\mathcal{L}_{(l)}$ as will be described later in Section 4.2.5.3.

4.2.5.2 Learning Transferability of Compounds

Inspired by the principle that similar compounds tend to bind to similar protein targets, our method identifies such similar compounds that have same activity labels across two targets, and hence learns compound-wise transferability. Given the scaled compound embedding \mathbf{z} of compound c , the compound-wise discriminator classifies whether the compound is from the source domain using a two-layer fully-connected neural network \mathbf{G} as follows,

$$q = \mathbf{G}(\mathbf{z}), \tag{10}$$

with ReLU at the hidden layer and sigmoid at the output layer. If q is very large or very small, c is very likely or very unlikely to belong to the source domain (it is equivalent to calculate the value with respect to the target domain, since there are only two domains to consider). If q is close to 0.5, c is likely to be common across domains (e.g., identical or similar compounds in the two domains) and thus can be used for information transfer across domains.

To learn the compound-wise discriminator, the loss function $\mathcal{L}_{(g)}$ is defined as follows,

$$\begin{aligned} \mathcal{L}_{(g)}(\Omega, \Psi) = & -\frac{1}{n^{(S)}} \sum_{\mathbf{x}^{(S)} \in \mathcal{X}^{(S)}} \log(q^{(S)}) \\ & -\frac{1}{n^{(T)}} \sum_{\mathbf{x}^{(T)} \in \mathcal{X}^{(T)}} \log(1 - q^{(T)}), \end{aligned} \tag{11}$$

where $n^{(S)}/n^{(T)}$ is the number of compounds in $\mathcal{X}^{(S)}/\mathcal{X}^{(T)}$ (i.e., $n = |\mathcal{D}|$); Ω and Ψ are learnable parameters of \mathbf{F} (compound representation learning network as in Section 4.2.2) and \mathbf{G} (Equation 10); and d is the dimension of compound feature embeddings. Note that in Equation 11, $q^{(S)}$ and $q^{(T)}$ represent the probability of $c^{(S)}$ and $c^{(T)}$ belonging to the *source domain*. Also, all the compounds from the source and target domains will be predicted using a same \mathbf{G} .

In order to identify similar compounds across domains, the discriminator needs to identify

compounds with their q values close to 0.5; when the q values are close 0.5, $\mathcal{L}_{(g)}$ will be maximized. Therefore, maximizing $\mathcal{L}_{(g)}$ will encourage more transferable compounds being learned and learned well. Meanwhile, to have an accurate compound-wise discriminator, compounds specific to the source/target domain should have large/small probabilities (i.e., large $q_i^{(S)}$ and small $q_i^{(T)}$) with respect to the source domain, and thus make the $\mathcal{L}_{(g)}$ value small. Therefore, minimizing $\mathcal{L}_{(g)}$ will encourage accurate probabilities. To combine these two aspects, similarly as to $\mathcal{L}_{(l)}$, an adversarial optimization will be applied to $\mathcal{L}_{(g)}$ as will be described later in Section 4.2.5.3.

According to \mathbf{G} , a compound that is common in the two domains, or is similar to compounds in the other domain, could be transferable (q value close to 0.5; not specific to source or target domain). However, such common or similar compounds may have different activity labels in the two domains. Using transferred information from common/similar compounds with conflicting labels in $\mathcal{T}^{(T)}$ will confuse any learners adversely. The compound-wise discriminator \mathbf{G} does not consider activity label information in learning compound transferability, and thus possibly induces conflicting information into $\mathcal{T}^{(T)}$. However, in the downstream domain-wise classification (Section 4.2.3), the minimization of domain-specific classification errors will prevent the transfer of conflicting information.

However, the input to the domain-wise classifier \mathbf{S} in TAc-fc is \mathbf{z} instead of \mathbf{r} as in Section 4.2.3. Given the scaled compound embedding \mathbf{z} , the domain-wise classifier classifies each compound in a given domain as active or inactive with respect to that domain using a two-layer fully-connected neural network \mathbf{S} as follows,

$$\hat{y} = \mathbf{S}(\mathbf{z}), \tag{12}$$

with ReLU at the hidden layer and sigmoid at the output layer. As discussed in Section 4.2.3, minimizing the loss $\mathcal{L}_{(c)}(\Omega, \Phi)$ enables correct classification in each domain, and prevent the transfer of conflicting information across domains.

4.2.5.3 TAc-fc Model Optimization

This section presents the optimization process of the proposed TAc-fc. TAc-fc constructs an end-to-end adversarial transfer learning framework with the above four components: 1) compound feature presentation learning network F , 2) feature-wise discriminator L , 3) compound-wise discriminator G , and 4) domain-wise classifier S . We solve for TAc-fc through optimizing the following loss function:

$$\mathcal{L}(\Omega, \Theta, \Psi, \Phi) = -\lambda[(\mathcal{L}_{(l)}(\Omega, \Theta) + \mathcal{L}_{(g)}(\Omega, \Psi))] + \mathcal{L}_{(c)}(\Omega, \Phi), \quad (13)$$

where Ω , Θ , Ψ and Φ are learnable parameters of F , L , G and S , respectively, and λ is a trade-off parameter. This loss function combines the three loss functions for L , G and S , and will be optimized in an adversarial way as follows:

(Step 1). Minimize \mathcal{L} with respect to Ω and Φ via solving the following optimization problem:

$$\widehat{\Omega}, \widehat{\Phi} = \arg \min_{\Omega, \Phi} \mathcal{L}(\Omega, \Theta, \Psi, \Phi). \quad (14)$$

By minimizing \mathcal{L} , we essentially minimize $\mathcal{L}_{(c)}$, and maximize $\mathcal{L}_{(l)}$ and $\mathcal{L}_{(g)}$. As discussed in L (Section 4.2.5.1) and G (Section 4.2.5.2), maximizing $\mathcal{L}_{(l)}$ and $\mathcal{L}_{(g)}$ will encourage learning of transferable features and compounds that can be used to help the tasks; as discussed in S (Section 4.2.3), minimizing $\mathcal{L}_{(c)}$ will prevent the transfer of conflicting information, in addition to minimizing the classification errors in each task.

(Step 2). Maximize \mathcal{L} with respect to Θ and Ψ via solving the following optimization problem:

$$\widehat{\Theta}, \widehat{\Psi} = \arg \max_{\Theta, \Psi} \mathcal{L}(\Omega, \Theta, \Psi, \Phi). \quad (15)$$

By maximizing \mathcal{L} , we essentially minimize $\mathcal{L}_{(l)}$ and $\mathcal{L}_{(g)}$ ($\mathcal{L}_{(c)}$ is fixed in this step). As discussed in L (Section 4.2.5.1) and G (Section 4.2.5.2), minimizing $\mathcal{L}_{(l)}$ and $\mathcal{L}_{(g)}$ will encourage that L and G accurately learn features and compounds that are specific to each domain so as to improve the classification performance of each domain.

(Step 3). The above two steps are iterated until the learning converges.

Thus, the optimization problem consists of a maximization with respect to some parameters and a minimization with respect to the others. In order to tackle such a mini-max optimization, we insert the gradient reversal layer (GRL)⁶⁴ between F and the discriminators L and G. GRL reverses the gradients during the backward propagation, and hence optimizes parameters Ω by maximizing the discriminator loss.

5 Acknowledgment

This project was made possible, in part, by support from the National Science Foundation under Grant Number IIS-1855501, IIS-1827472 and IIS-2133650, and AWS Machine Learning Research Award. Any opinions, findings, and conclusions or recommendations expressed in this material are those of the authors and do not necessarily reflect the views of the funding agencies.

References

- (1) Dickson, M.; Gagnon, J. P. The cost of new drug discovery and development. *Discov. Med.* **2009**, *4*, 172–179.
- (2) DiMasi, J. A.; Hansen, R. W.; Grabowski, H. G. The price of innovation: New estimates of drug development costs. *J. Health Econ.* **2003**, *22*, 151–185.
- (3) Terstappen, G. C.; Reggiani, A. In silico research in drug discovery. *Trends Pharmacol. Sci.* **2001**, *22*, 23–26.
- (4) Sliwoski, G.; Kothiwale, S.; Meiler, J.; Lowe, E. W. Computational methods in drug discovery. *Pharmacol. Rev.* **2014**, *66*, 334–395.
- (5) Hansch, C.; Maloney, P. P.; Fujita, T.; Muir, R. M. Correlation of biological activity

- of phenoxyacetic acids with Hammett substituent constants and partition coefficients. *Nature* **1962**, *194*, 178–180.
- (6) Debnath, A. K.; Lopez de Compadre, R. L.; Debnath, G.; Shusterman, A. J.; Hansch, C. Structure-activity relationship of mutagenic aromatic and heteroaromatic nitro compounds. Correlation with molecular orbital energies and hydrophobicity. *J. Med. Chem.* **1991**, *34*, 786–797.
- (7) Superti-Furga, G.; Courtneidge, S. A. Structure-function relationships in Src family and related protein tyrosine kinases. *BioEssays* **1995**, *17*, 321–330.
- (8) Dudek, A.; Arodz, T.; Galvez, J. Computational methods in developing quantitative structure-activity relationships (QSAR): a review. *Comb. Chem. High Throughput Screening* **2006**, *9*, 213–228.
- (9) Imrie, F.; Bradley, A. R.; Van Der Schaar, M.; Deane, C. M. Protein family-specific models using deep neural networks and transfer learning improve virtual screening and highlight the need for more data. *J. Chem. Inf. Model.* **2018**, *58*, 2319–2330.
- (10) Ning, X.; Rangwala, H.; Karypis, G. Multi-assay-based structure-activity relationship models: Improving structure-activity relationship models by incorporating activity information from related targets. *J. Chem. Inf. Model.* **2009**, *49*, 2444–2456.
- (11) Liu, J.; Ning, X. Multi-assay-based compound prioritization via assistance utilization: a machine learning framework. *J. Chem. Inf. Model.* **2017**, *57*, 484–498.
- (12) Liu, J.; Ning, X. Differential compound prioritization via bidirectional selectivity push with power. *J. Chem. Inf. Model.* **2017**, *57*, 2958–2975.
- (13) Murcko, M. Chemogenomic approaches to drug discovery. *Curr. Opin. Chem. Biol.* **2001**, *5*, 464–470.

- (14) Kubinyi, H.; Müller, G. *Chemogenomics in Drug Discovery: A Medicinal Chemistry Perspective*; Wiley, 2005.
- (15) Harris, C. J.; Stevens, A. P. Chemogenomics: structuring the drug discovery process to gene families. *Drug Discovery Today* **2006**, *11*, 880–888.
- (16) Klabunde, T. Chemogenomic approaches to drug discovery: Similar receptors bind similar ligands. *Br. J. Pharmacol.* **2007**, *152*, 5–7.
- (17) Pan, S. J.; Yang, Q. A survey on transfer learning. *IEEE Trans. Knowl. Data Eng.* **2010**, *22*, 1345–1359.
- (18) Cai, C.; Wang, S.; Xu, Y.; Zhang, W.; Tang, K.; Ouyang, Q.; Lai, L.; Pei, J. Transfer learning for drug discovery. *J. Med. Chem.* **2020**, *63*, 8683–8694.
- (19) Yang, K.; Swanson, K.; Jin, W.; Coley, C.; Eiden, P.; Gao, H.; Guzman-Perez, A.; Hopper, T.; Kelley, B.; Mathea, M.; Palmer, A.; Settels, V.; Jaakkola, T.; Jensen, K.; Barzilay, R. Analyzing learned molecular representations for property prediction. *J. Chem. Inf. Model.* **2019**, *59*, 3370–3388.
- (20) Kim, S.; Chen, J.; Cheng, T.; Gindulyte, A.; He, J.; He, S.; Li, Q.; Shoemaker, B. A.; Thiessen, P. A.; Yu, B.; Zaslavsky, L.; Zhang, J.; Bolton, E. E. PubChem in 2021: New data content and improved web interfaces. *Nucleic Acids Res.* **2020**, *49*, 388–395.
- (21) ur Rahman, A.; Choudhary, M. I.; Thomsen, W. J. *Bioassay techniques for drug development*; CRC Press, 2001.
- (22) Tareq Hassan Khan, M. Predictions of the ADMET properties of candidate drug molecules utilizing different QSAR/QSPR modelling approaches. *Curr. Drug Metab.* **2010**, *11*, 285–295.
- (23) Lo, Y. C.; Rensi, S. E.; Torng, W.; Altman, R. B. Machine learning in chemoinformatics and drug discovery. *Drug Discovery Today* **2018**, *23*, 1538–1546.

- (24) Interpretation of quantitative structure - property and - activity relationships. *J. Chem. Inf. Comput. Sci.* **2001**, *41*, 679–685.
- (25) Czermiski, R.; Yasri, A.; Hartsough, D. Use of support vector machine in pattern classification: Application to QSAR studies. *Quant. Struct.-Act. Relat.* **2001**, *20*, 227–240.
- (26) Zernov, V. V.; Balakin, K. V.; Ivaschenko, A. A.; Savchuk, N. P.; Pletnev, I. V. Drug discovery using support vector machines. The case studies of drug-likeness, agrochemical-likeness, and enzyme inhibition predictions. *J. Chem. Inf. Comput. Sci.* **2003**, *43*, 2048–2056.
- (27) Hou, T.; Wang, J.; Li, Y. ADME evaluation in drug discovery. 8. The prediction of human intestinal absorption by a support vector machine. *J. Chem. Inf. Model.* **2007**, *47*, 2408–2415.
- (28) Alvarsson, J.; Lampa, S.; Schaal, W.; Andersson, C.; Wikberg, J. E.; Spjuth, O. Large-scale ligand-based predictive modelling using support vector machines. *J. Cheminf.* **2016**, *8*, 1–9.
- (29) Svetnik, V.; Liaw, A.; Tong, C.; Christopher Culberson, J.; Sheridan, R. P.; Feuston, B. P. Random forest: a classification and regression tool for compound classification and QSAR modeling. *J. Chem. Inf. Comput. Sci.* **2003**, *43*, 1947–1958.
- (30) Zhang, Q. Y.; Aires-de Sousa, J. Random forest prediction of mutagenicity from empirical physicochemical descriptors. *J. Chem. Inf. Model.* **2007**, *47*, 1–8.
- (31) Xia, X.; Maliski, E. G.; Gallant, P.; Rogers, D. Classification of kinase inhibitors using a Bayesian model. *J. Med. Chem.* **2004**, *47*, 4463–4470.
- (32) Chen, L.; Li, Y.; Zhao, Q.; Peng, H.; Hou, T. ADME evaluation in drug discovery. 10.

- Predictions of P-glycoprotein inhibitors using recursive partitioning and naive bayesian classification techniques. *Mol. Pharmaceutics* **2011**, *8*, 889–900.
- (33) Rogers, D.; Hahn, M. Extended-connectivity fingerprints. *J. Chem. Inf. Model.* **2010**, *50*, 742–754.
- (34) Durant, J. L.; Leland, B. A.; Henry, D. R.; Nourse, J. G. Reoptimization of MDL keys for use in drug discovery. *J. Chem. Inf. Comput. Sci.* **2002**, *42*, 1273–1280.
- (35) Randić, M. Novel molecular descriptor for structure-property studies. *Chem. Phys. Lett.* **1993**, *211*, 478–483.
- (36) Ma, J.; Sheridan, R. P.; Liaw, A.; Dahl, G. E.; Svetnik, V. Deep neural nets as a method for quantitative structure-activity relationships. *J. Chem. Inf. Model.* **2015**, *55*, 263–274.
- (37) Gawehn, E.; Hiss, J. A.; Schneider, G. Deep learning in drug discovery. *Mol. Inf.* **2016**, *35*, 3–14.
- (38) Zhang, L.; Tan, J.; Han, D.; Zhu, H. From machine learning to deep learning: progress in machine intelligence for rational drug discovery. *Drug Discovery Today* **2017**, *22*, 1680–1685.
- (39) Chen, H.; Engkvist, O.; Wang, Y.; Olivecrona, M.; Blaschke, T. The rise of deep learning in drug discovery. *Drug Discovery Today* **2018**, *23*, 1241–1250.
- (40) Hop, P.; Allgood, B.; Yu, J. Geometric deep learning autonomously learns chemical features that outperform those engineered by domain experts. *Mol. Pharmaceutics* **2018**, *15*, 4371–4377.
- (41) Klambauer, G.; Unterthiner, T.; Mayr, A.; Hochreiter, S. DeepTox: Toxicity prediction using deep learning. *Toxicol. Lett.* **2017**, *280*, S69.

- (42) Wenzel, J.; Matter, H.; Schmidt, F. Predictive multitask deep neural network models for ADME-Tox properties: Learning from Large Data Sets. *J. Chem. Inf. Model.* **2019**, *59*, 1253–1268.
- (43) Wu, Z.; Lei, T.; Shen, C.; Wang, Z.; Cao, D.; Hou, T. ADMET evaluation in drug discovery. 19. Reliable prediction of human Cytochrome P450 inhibition using artificial intelligence approaches. *J. Chem. Inf. Model.* **2019**, *59*, 4587–4601.
- (44) Duvenaud, D. K.; Maclaurin, D.; Iparraguirre, J.; Bombarell, R.; Hirzel, T.; Aspuru-Guzik, A.; Adams, R. P. Convolutional networks on graphs for learning molecular fingerprints. *Advances in Neural Information Processing Systems*. 2015; pp 2224–2232.
- (45) Kearnes, S.; McCloskey, K.; Berndl, M.; Pande, V.; Riley, P. Molecular graph convolutions: moving beyond fingerprints. *J. Comput.-Aided Mol. Des.* **2016**, *30*, 595–608.
- (46) Gilmer, J.; Schoenholz, S. S.; Riley, P. F.; Vinyals, O.; Dahl, G. E. Neural message passing for quantum chemistry. *International Conference on Machine Learning*. 2017; pp 1263–1272.
- (47) Sun, M.; Zhao, S.; Gilvary, C.; Elemento, O.; Zhou, J.; Wang, F. Graph convolutional networks for computational drug development and discovery. *Briefings Bioinf.* **2020**, *21*, 919–935.
- (48) Withnall, M.; Lindelöf, E.; Engkvist, O.; Chen, H. Building attention and edge message passing neural networks for bioactivity and physical-chemical property prediction. *J. Cheminf.* **2020**, *12*, 1–18.
- (49) Zheng, S.; Yan, X.; Yang, Y.; Xu, J. Identifying structure–property relationships through SMILES syntax analysis with self-attention mechanism. *J. Chem. Inf. Model.* **2019**, *59*, 914–923.

- (50) Chakravarti, S. K.; Alla, S. R. M. Descriptor free QSAR modeling using deep learning with long short-term memory neural networks. *Front. Artif. Intell.* **2019**, *2*, 17.
- (51) Karpov, P.; Godin, G.; Tetko, I. V. Transformer-CNN: Swiss knife for QSAR modeling and interpretation. *J. Cheminf.* **2020**, *12*, 1–12.
- (52) Tan, C.; Sun, F.; Kong, T.; Zhang, W.; Yang, C.; Liu, C. A survey on deep transfer learning. International Conference on Artificial Neural Networks. 2018; pp 270–279.
- (53) Zhuang, F.; Qi, Z.; Duan, K.; Xi, D.; Zhu, Y.; Zhu, H.; Xiong, H.; He, Q. A comprehensive survey on transfer learning. *Proc. IEEE* **2021**, *109*, 43–76.
- (54) Yosinski, J.; Clune, J.; Bengio, Y.; Lipson, H. How transferable are features in deep neural networks? Advances in Neural Information Processing Systems. 2014; pp 3320–3328.
- (55) Wang, Z.; Dai, Z.; Póczos, B.; Carbonell, J. Characterizing and avoiding negative transfer. IEEE Conference on Computer Vision and Pattern Recognition. 2019; pp 11285–11294.
- (56) Pan, S. J.; Tsang, I. W.; Kwok, J. T.; Yang, Q. Domain adaptation via transfer component analysis. *IEEE Trans. Neural Netw.* **2011**, *22*, 199–210.
- (57) Long, M.; Wang, J.; Ding, G.; Sun, J.; Yu, P. S. Transfer feature learning with joint distribution adaptation. IEEE International Conference on Computer Vision. 2013; pp 2200–2207.
- (58) Wang, M.; Deng, W. Deep visual domain adaptation: A survey. *Neurocomputing* **2018**, *312*, 135–153.
- (59) Tzeng, E.; Hoffman, J.; Zhang, N.; Saenko, K.; Darrell, T. Deep domain confusion: Maximizing for domain invariance. *CoRR* **2014**, *abs/1412.3474*.

- (60) Long, M.; Cao, Y.; Wang, J.; Jordan, M. I. Learning transferable features with deep adaptation networks. International Conference on Machine Learning. Lille, France, 2015; pp 97–105.
- (61) Long, M.; Zhu, H.; Wang, J.; Jordan, M. I. Unsupervised domain adaptation with residual transfer networks. Advances in Neural Information Processing Systems. 2016; pp 136–144.
- (62) Liu, H.; Long, M.; Wang, J.; Jordan, M. I. Transferable adversarial training: A general approach to adapting deep classifiers. International Conference on Machine Learning. 2019; pp 4013–4022.
- (63) Goodfellow, I. J.; Pouget-Abadie, J.; Mirza, M.; Xu, B.; Warde-Farley, D.; Ozair, S.; Courville, A.; Bengio, Y. Generative adversarial nets. Advances in Neural Information Processing Systems. 2014; pp 2672–2680.
- (64) Ganin, Y.; Lempitsky, V. Unsupervised domain adaptation by backpropagation. International Conference on Machine Learning. Lille, France, 2015; pp 1180–1189.
- (65) Long, M.; Zhu, H.; Wang, J.; Jordan, M. I. Deep transfer learning with joint adaptation networks. International Conference on Machine Learning. 2017; pp 2208–2217.
- (66) Sankaranarayanan, S.; Balaji, Y.; Castillo, C. D.; Chellappa, R. Generate to adapt: Aligning domains using generative adversarial networks. IEEE Conference on Computer Vision and Pattern Recognition. 2018; pp 8503–8512.
- (67) Tzeng, E.; Hoffman, J.; Saenko, K.; Darrell, T. Adversarial discriminative domain adaptation. IEEE Conference on Computer Vision and Pattern Recognition. 2017.
- (68) Long, M.; Cao, Z.; Wang, J.; Jordan, M. I. Conditional adversarial domain adaptation. Advances in Neural Information Processing Systems. 2018; pp 1640–1650.

- (69) Monteiro, J.; Gibert, X.; Feng, J.; Dumoulin, V.; Lee, D.-S. Domain conditional predictors for domain adaptation. *Proc. Mach. Learn. Res.* **2021**, *148*, 193–220.
- (70) Pei, Z.; Cao, Z.; Long, M.; Wang, J. Multi-adversarial domain adaptation. AAAI Conference on Artificial Intelligence. 2018.
- (71) Zhao, H.; Zhang, S.; Wu, G.; Costeira, J. P.; Moura, J. M.; Gordon, G. J. Multiple source domain adaptation with adversarial learning. International Conference on Learning Representations - Workshop Track Proceedings. 2018.
- (72) Altae-Tran, H.; Ramsundar, B.; Pappu, A. S.; Pande, V. Low data drug discovery with one-shot learning. *ACS Cent. Sci.* **2017**, *3*, 283–293.
- (73) Simões, R. S.; Maltarollo, V. G.; Oliveira, P. R.; Honorio, K. M. Transfer and multi-task learning in QSAR modeling: Advances and challenges. *Front. Pharmacol.* **2018**, *9*.
- (74) Lee, M.; Kim, H.; Joe, H.; Kim, H. G. Multi-channel PINN: Investigating scalable and transferable neural networks for drug discovery. *J. Cheminf.* **2019**, *11*, 1–16.
- (75) Guo, Z.; Zhang, C.; Yu, W.; Herr, J.; Wiest, O.; Jiang, M.; Chawla, N. V. Few-shot graph learning for molecular property prediction. Web Conference 2021. New York, NY, USA, 2021; pp 2559–2567.
- (76) Dahl, G. E.; Jaitly, N.; Salakhutdinov, R. Multi-task neural networks for QSAR predictions. *CoRR* **2014**, *abs/1406.1231*.
- (77) Ramsundar, B.; Liu, B.; Wu, Z.; Verras, A.; Tudor, M.; Sheridan, R. P.; Pande, V. Is multitask deep learning practical for pharma? *J. Chem. Inf. Model.* **2017**, *57*, 2068–2076.
- (78) Demystifying multitask deep neural networks for quantitative structure–activity relationships. *J. Chem. Inf. Model.* **2017**, *57*, 2490–2504.

- (79) Rodríguez-Pérez, R.; Bajorath, J. Multitask machine learning for classifying highly and weakly potent kinase inhibitors. *ACS Omega* **2019**, *4*, 4367–4375.
- (80) Sosnin, S.; Vashurina, M.; Withnall, M.; Karpov, P.; Fedorov, M.; Tetko, I. V. A survey of multi-task learning methods in chemoinformatics. *Mol. Inf.* **2019**, *38*, 1800108.
- (81) Goh, G. B.; Siegel, C.; Vishnu, A.; Hodas, N. Using rule-based labels for weak supervised learning: a ChemNet for transferable chemical property prediction. ACM SIGKDD International Conference on Knowledge Discovery & Data Mining. New York, NY, USA, 2018; p 302–310.
- (82) Li, X.; Fourches, D. Inductive transfer learning for molecular activity prediction: Next-gen QSAR models with MolPMoFiT. *J. Cheminf.* **2020**, *12*, 1–15.
- (83) Hochreiter, S.; Schmidhuber, J. Long short-term memory. *Neural Comput.* **1997**, *9*, 1735–1780.
- (84) Abbasi, K.; Poso, A.; Ghasemi, J.; Amanlou, M.; Masoudi-Nejad, A. Deep transferable compound representation across domains and tasks for low data drug discovery. *J. Chem. Inf. Model.* **2019**, *59*, 4528–4539.
- (85) Kim, S.; Chen, J.; Cheng, T.; Gindulyte, A.; He, J.; He, S.; Li, Q.; Shoemaker, B. A.; Thiessen, P. A.; Yu, B.; Zaslavsky, L.; Zhang, J.; Bolton, E. E. PubChem 2019 update: Improved access to chemical data. *Nucleic Acids Res.* **2018**, *47*, 102–109.
- (86) Bateman, A. et al. UniProt: The universal protein knowledgebase in 2021. *Nucleic Acids Res.* **2021**, *49*, 480–489.
- (87) Santos, R.; Ursu, O.; Gaulton, A.; Bento, A. P.; Donadi, R. S.; Bologa, C. G.; Karlsson, A.; Al-Lazikani, B.; Hersey, A.; Oprea, T. I.; Overington, J. P. A comprehensive map of molecular drug targets. *Nat. Rev. Drug Discovery* **2016**, *16*, 19–34.

- (88) Zdrazil, B.; Richter, L.; Brown, N.; Guha, R. Moving targets in drug discovery. *Sci. Rep.* **2020**, *10*, 1–15.
- (89) Willett, P.; Barnard, J. M.; Downs, G. M. Chemical similarity searching. *J. Chem. Inf. Comput. Sci.* **1998**, *38*, 983–996.
- (90) Landrum, G. RDKit: open-source cheminformatics software. 2020; <https://www.rdkit.org>, (accessed 2020-01-22).
- (91) Wang, X.; Gao, J.; Long, M.; Wang, J. Self-tuning for data-efficient deep learning. International Conference on Machine Learning. 2021; pp 10738–10748.
- (92) Kingma, D. P.; Ba, J. L. Adam: A method for stochastic optimization. International Conference on Learning Representations. 2015.
- (93) Wu, Z.; Ramsundar, B.; Feinberg, E. N.; Gomes, J.; Geniesse, C.; Pappu, A. S.; Leswing, K.; Pande, V. MoleculeNet: A benchmark for molecular machine learning. *Chem. Sci.* **2018**, *9*, 513–530.
- (94) Descriptor computation(chemistry) and (optional) storage for machine learning. <https://github.com/bp-kelley/descriptastorus>, (accessed 2020-08-10).
- (95) Scarselli, F.; Gori, M.; Tsoi, A. C.; Hagenbuchner, M.; Monfardini, G. The graph neural network model. *IEEE Trans. Neural Netw.* **2009**, *20*, 61–80.
- (96) Veličković, P.; Casanova, A.; Liò, P.; Cucurull, G.; Romero, A.; Bengio, Y. Graph attention networks. *CoRR* **2018**, *abs/1710.10903*.

Improving Compound Activity Classification via Deep Transfer and Representation Learning (Supplementary Materials)

Vishal Dey,[†] Raghu Machiraju,^{†,‡,¶} and Xia Ning^{*,†,‡,¶}

[†]*Department of Computer Science and Engineering, The Ohio State University, Columbus,
OH*

[‡]*Biomedical Informatics, The Ohio State University, Columbus, OH*

[¶]*Translational Data Analytics Institute, The Ohio State University, Columbus, OH*

E-mail: ning.104@osu.edu

1 Directed Message Passing Neural Networks

dmpn incorporates atom features \mathbf{a}_u for each atom $u \in \mathcal{A}_c$ and bond features \mathbf{e}_{uv} for each bond $(u, v) \in \mathcal{E}_c$, and captures molecular substructures by propagating messages along directed edges in \mathcal{G}_c . **dmpn** initializes atom features \mathbf{a}_u using the atom’s physicochemical properties including mass, formal charge, chirality, type, number of connected bonds, etc. **dmpn** initializes bond features \mathbf{e}_{uv} using bond type, stereo configuration, etc.

In particular, in \mathcal{G}_c , each bond (u, v) is associated with two messages \mathbf{m}_{uv} and \mathbf{m}_{vu} encoding messages from atom u to v and vice versa. Each message $\mathbf{m}_{uv}^{(t+1)}$ in the $(t + 1)$ -th

iteration of `dmpn` is aggregated as follows,

$$\mathbf{m}_{uv}^{(t+1)} = \sum_{k \in \mathcal{N}(u) \setminus v} \mathbf{h}_{ku}^{(t)} \quad (1)$$

where $\mathcal{N}(u)$ is the set of atoms connected to u , $\mathbf{h}_{ku}^{(t)}$ is the hidden state of edge (k, u) in the t -th iteration. In the $(t + 1)$ -th iteration of message passing, the hidden state $\mathbf{h}_{uv}^{(t+1)}$ for each edge (u, v) is updated as follows,

$$\mathbf{h}_{uv}^{(t+1)} = \text{ReLU}(\mathbf{h}_{uv}^{(0)} + W\mathbf{m}_{uv}^{(t+1)}), \quad (2)$$

where W is a learnable parameter matrix, and $\mathbf{h}_{uv}^{(0)}$ is the initial hidden state of edge (u, v) initialized as follows,

$$\mathbf{h}_{uv}^{(0)} = \text{ReLU}(W_0[\mathbf{a}_u, \mathbf{e}_{uv}]) \quad (3)$$

where \mathbf{a}_u and \mathbf{e}_{uv} are atom and bond feature vectors, respectively, $[\mathbf{a}_u, \mathbf{e}_{uv}]$ is the concatenation of \mathbf{a}_u and \mathbf{e}_{uv} and W_0 is a learnable parameter.

After the final iteration of message passing, the hidden states for edges incident to an atom u are aggregated to generate an intermediate representation \mathbf{h}_u for that atom as follows,

$$\mathbf{h}_u = \sum_{k \in \mathcal{N}(u)} \mathbf{h}_{ku}^{(\tau)}, \quad (4)$$

where τ is the total number of message passing iterations. These intermediate atom representations are then used to generate another atom representation that also incorporates atom features \mathbf{a}_u as follows,

$$\mathbf{s}_u = \text{ReLU}(W_e[\mathbf{a}_u, \mathbf{h}_u]), \quad (5)$$

where W_e is a learnable parameter and $[\mathbf{a}_u, \mathbf{h}_u]$ is the concatenation of \mathbf{a}_u and \mathbf{h}_u . Thus, the atom representation \mathbf{h}_u captures structural information about atom u 's τ -hop neighbors, thereby enhancing the representation power. Given the representation \mathbf{h}_u for each atom in

c , `dmpn` produces an embedding for c using mean pooling over all the atom representations as follows,

$$\mathbf{r}_c = \frac{1}{|\mathcal{A}_c|} \sum_{u \in \mathcal{A}_c} \mathbf{s}_u, \quad (6)$$

where $|\mathcal{A}_c|$ is the number of atoms in c .

2 Supplementary Materials

2.1 Assay Information

Table S1 presents the assay statistics of 93 processed bioassays with their associated target protein accession IDs in PubChem; their number of total, active and inactive compounds, and the corresponding protein family for each associated target.

Table S1: Compound statistics of processed bioassays

protacxn	#total	# active	# inactive	Protein family
NP_001017535	380,711	5,152	375,559	Nuclear hormone receptor family
AAH18745	374,923	1,230	373,693	Peptidase family
NP_005021	349,900	10,198	339,702	Protein kinase superfamily
NP_004196	336,578	238	336,340	Peptidase family
NP_057051	292,415	97	292,318	Protein-tyrosine phosphatase family
NP_000903	292,382	151	292,231	G-protein coupled receptor 1 family
NP_005292	292,044	207	291,837	G-protein coupled receptor 1 family
NP_004081	290,998	1,674	289,324	Protein-tyrosine phosphatase family
NP_001121649	275,994	116	275,878	Nuclear hormone receptor family
NP_997055	208,843	2,526	206,317	G-protein coupled receptor 1 family
NP_002736	182,123	1,207	180,916	Protein kinase superfamily

Continued on next page

Table S1 – continued from previous page

protacxn	#total	# active	# inactive	Protein family
NP_542155	112,687	906	111,781	Protein-tyrosine phosphatase family
NP_775180	96,456	153	96,303	Nuclear hormone receptor family
P55210	71,790	77	71,713	Peptidase family
NP_150634	70,986	61	70,925	Peptidase family
NP_000483	10,100	179	9,921	ABC transporter superfamily
ABB72139	6,968	64	6,904	Nuclear hormone receptor family
ADZ17337	6,738	86	6,652	Nuclear hormone receptor family
NP_000762	7,759	1,163	6,596	Cytochrome P450 family
EAW77416	7,131	626	6,505	Cytochrome P450 family
ADZ17384	6,425	55	6,370	Nuclear hormone receptor family
NP_000760	7,676	1,713	5,963	Cytochrome P450 family
NP_000752	7,670	4,008	3,662	Cytochrome P450 family
AAF64255	2,728	1,107	1,621	Bcl-2 family
NP_002084	2,285	682	1,603	Protein kinase superfamily
NP_063937	2,390	823	1,567	Protein kinase superfamily
AAI28575	1,824	305	1,519	Nuclear hormone receptor family
AAB26273	1,669	276	1,393	G-protein coupled receptor 1 family
NP_000947	1,350	139	1,211	G-protein coupled receptor 1 family
NP_036559	1,260	109	1,151	Peptidase family
NP_065717	1,630	661	969	Protein kinase superfamily
AAI27629	1,065	160	905	G-protein coupled receptor 1 family
P51449	978	138	840	Nuclear hormone receptor family
NP_004040	824	91	733	Bcl-2 family

Continued on next page

Table S1 – continued from previous page

protacxn	#total	# active	# inactive	Protein family
P00748	761	160	601	Peptidase family
ABD72211	1,164	605	559	ABC transporter superfamily
AAH04460	993	445	548	Peptidase family
NP_004950	954	456	498	Nuclear hormone receptor family
NP_000676	667	209	458	G-protein coupled receptor 1 family
NP_000466	489	55	434	Nuclear hormone receptor family
NP_005152	672	259	413	G-protein coupled receptor 1 family
NP_001391	729	345	384	G-protein coupled receptor 1 family
NP_005217	456	82	374	G-protein coupled receptor 1 family
NP_660205	1,167	795	372	Peptidase family
NP_000789	457	100	357	G-protein coupled receptor 1 family
NP_001027450	543	203	340	Peptidase family
NP_004521	445	107	338	Peptidase family
NP_004960	387	61	326	Peptidase family
NP_005424	693	368	325	Protein kinase superfamily
P53779	362	57	305	Protein kinase superfamily
AAC63054	517	223	294	Peptidase family
AAF04852	973	683	290	Peptidase family
NP_004337	1,055	781	274	Peptidase family
AAA51985	366	105	261	Peptidase family
NP_004358	289	58	231	G-protein coupled receptor 1 family
NP_004221	276	69	207	G-protein coupled receptor 1 family
NP_000901	292	88	204	G-protein coupled receptor 1 family

Continued on next page

Table S1 – continued from previous page

protacxn	#total	# active	# inactive	Protein family
NP_002522	349	156	193	G-protein coupled receptor 1 family
NP_644806	248	57	191	Peptidase family
EAW86722	539	350	189	G-protein coupled receptor 1 family
NP_000900	291	104	187	G-protein coupled receptor 1 family
AAI07736	242	59	183	Bcl-2 family
AAI29989	981	799	182	Peptidase family
BAH02301	462	317	145	Nuclear hormone receptor family
NP_000448	292	149	143	Nuclear hormone receptor family
NP_004841	229	88	141	Protein kinase superfamily
AAH14970	248	126	122	G-protein coupled receptor 1 family
NP_002721	190	71	119	Protein kinase superfamily
NP_003813	211	92	119	Nuclear hormone receptor family
AAH36651	210	92	118	Protein kinase superfamily
Q05397	210	110	100	Protein kinase superfamily
NP_004570	151	52	99	Protein kinase superfamily
NP_000918	189	102	87	ABC transporter superfamily
NP_112168	304	217	87	Protein kinase superfamily
NP_066285	233	173	60	Nuclear hormone receptor family
BAB91222	142	91	51	G-protein coupled receptor 1 family
NP_003605	232	181	51	G-protein coupled receptor 1 family
P28566	95	51	44	G-protein coupled receptor 1 family
NP_037457	331	290	41	Peptidase family
Q6L5J4	432	391	41	G-protein coupled receptor 1 family

Continued on next page

Table S1 – continued from previous page

protacxn	#total	# active	# inactive	Protein family
NP_000732	98	58	40	G-protein coupled receptor 1 family
NP_612200	314	274	40	G-protein coupled receptor 1 family
NP_001387	307	270	37	Protein kinase superfamily
NP_004818	125	89	36	ABC transporter superfamily
EAW70217	188	154	34	Protein kinase superfamily
AAH14460	91	69	22	Peptidase family
NP_001124480	81	64	17	Protein-tyrosine phosphatase family
NP_001516	171	156	15	G-protein coupled receptor 1 family
NP_003984	95	83	12	Protein kinase superfamily
NP_004705	94	82	12	Protein kinase superfamily
NP_004062	96	88	8	Protein kinase superfamily
NP_002825	166	160	6	Protein-tyrosine phosphatase family
NP_004942	74	69	5	G-protein coupled receptor 1 family

In this table, the columns protacxn, #total, #active and #inactive correspond to the target protein’s accession number from PubChem, number of total compounds, active compounds and inactive compounds in the bioassay, respectively. The column Protein family denotes the corresponding protein family for each target.

2.2 Assay Pairs Information

Table S2 presents the compound statistics of all 120 pairs in \mathcal{P} with their number of total, active and inactive compounds in each assay of every pair.

Table S2: Compound statistics of selected bioassay pairs

target(P)	target(Q)	$ \mathcal{X}_{B_P} $	$ \mathcal{X}_{B_P}^+ $	$ \mathcal{X}_{B_P}^- $	$ \mathcal{X}_{B_Q} $	$ \mathcal{X}_{B_Q}^+ $	$ \mathcal{X}_{B_Q}^- $
NP_005021	NP_004705	20,396	10,198	10,198	164	82	82
NP_000903	EAW86722	302	151	151	666	333	333
NP_000903	BAB91222	302	151	151	166	83	83
NP_005292	BAB91222	414	207	207	166	83	83
NP_005292	NP_004942	414	207	207	134	67	67
NP_004081	NP_002825	3,288	1,644	1,644	248	124	124
NP_997055	NP_004942	5,052	2,526	2,526	134	67	67
NP_775180	ADZ17337	306	153	153	170	85	85
NP_000483	ABD72211	356	178	178	1,188	594	594
NP_000483	NP_000918	358	179	179	204	102	102
NP_000483	NP_004818	358	179	179	178	89	89
ADZ17337	AAI28575	156	78	78	592	296	296
ADZ17337	NP_000448	172	86	86	298	149	149
ADZ17337	NP_066285	172	86	86	342	171	171
NP_000762	NP_000752	888	444	444	1,918	959	959
NP_000760	NP_000752	1,356	678	678	2,070	1,035	1,035
NP_002084	P53779	1,358	679	679	112	56	56
AAI28575	P51449	608	304	304	244	122	122
AAI28575	BAH02301	608	304	304	626	313	313
AAI28575	NP_000448	608	304	304	298	149	149
AAI28575	NP_066285	610	305	305	346	173	173
AAB26273	NP_000947	536	268	268	272	136	136
AAB26273	AAI27629	552	276	276	320	160	160

Continued on next page

Table S2 – continued from previous page

target(P)	target(Q)	$ \mathcal{X}_{B_P} $	$ \mathcal{X}_{B_P}^+ $	$ \mathcal{X}_{B_P}^- $	$ \mathcal{X}_{B_Q} $	$ \mathcal{X}_{B_Q}^+ $	$ \mathcal{X}_{B_Q}^- $
AAB26273	NP_000676	552	276	276	416	208	208
AAB26273	NP_001391	548	274	274	688	344	344
AAB26273	NP_004358	552	276	276	116	58	58
AAB26273	NP_000901	552	276	276	174	87	87
AAB26273	EAW86722	552	276	276	700	350	350
AAB26273	NP_000900	552	276	276	206	103	103
AAB26273	AAH14970	552	276	276	252	126	126
AAB26273	BAB91222	552	276	276	182	91	91
AAB26273	NP_003605	552	276	276	360	180	180
AAB26273	NP_612200	552	276	276	542	271	271
AAB26273	NP_001516	552	276	276	310	155	155
NP_000947	AAI27629	278	139	139	318	159	159
NP_000947	EAW86722	278	139	139	700	350	350
NP_000947	BAB91222	278	139	139	182	91	91
NP_000947	NP_001516	278	139	139	308	154	154
NP_036559	P00748	168	84	84	274	137	137
NP_036559	AAC63054	184	92	92	410	205	205
NP_036559	AAF04852	218	109	109	1,362	681	681
NP_036559	NP_004337	218	109	109	1,556	778	778
NP_036559	AAA51985	174	87	87	180	90	90
NP_036559	AAI29989	218	109	109	1,592	796	796
NP_036559	AAH14460	202	101	101	120	60	60
NP_065717	NP_001387	1,028	514	514	278	139	139

Continued on next page

Table S2 – continued from previous page

target(P)	target(Q)	$ \mathcal{X}_{B_P} $	$ \mathcal{X}_{B_P}^+ $	$ \mathcal{X}_{B_P}^- $	$ \mathcal{X}_{B_Q} $	$ \mathcal{X}_{B_Q}^+ $	$ \mathcal{X}_{B_Q}^- $
NP_065717	EAW70217	1,268	634	634	260	130	130
AAI27629	EAW86722	320	160	160	698	349	349
AAI27629	NP_004942	320	160	160	138	69	69
P00748	NP_660205	320	160	160	1,586	793	793
P00748	NP_004521	320	160	160	214	107	107
P00748	AAC63054	266	133	133	382	191	191
P00748	AAF04852	320	160	160	1,364	682	682
P00748	NP_004337	320	160	160	1,558	779	779
P00748	AAA51985	244	122	122	154	77	77
P00748	AAI29989	320	160	160	1,596	798	798
P00748	AAH14460	296	148	148	114	57	57
ABD72211	NP_000918	1,210	605	605	202	101	101
ABD72211	NP_004818	1,210	605	605	178	89	89
AAH04460	AAH14460	890	445	445	138	69	69
NP_000676	NP_005152	154	77	77	172	86	86
NP_000676	NP_000901	416	208	208	176	88	88
NP_000676	EAW86722	418	209	209	700	350	350
NP_000676	NP_001516	418	209	209	310	155	155
NP_000676	NP_004942	418	209	209	138	69	69
NP_005152	NP_004358	512	256	256	108	54	54
NP_005152	NP_001516	518	259	259	310	155	155
NP_001391	NP_000901	682	341	341	174	87	87
NP_001391	EAW86722	690	345	345	700	350	350

Continued on next page

Table S2 – continued from previous page

target(P)	target(Q)	$ \mathcal{X}_{B_P} $	$ \mathcal{X}_{B_P}^+ $	$ \mathcal{X}_{B_P}^- $	$ \mathcal{X}_{B_Q} $	$ \mathcal{X}_{B_Q}^+ $	$ \mathcal{X}_{B_Q}^- $
NP_001391	NP_000900	682	341	341	206	103	103
NP_001391	BAB91222	690	345	345	182	91	91
NP_001391	NP_001516	690	345	345	308	154	154
NP_660205	NP_004337	914	457	457	642	321	321
NP_660205	AAI29989	986	493	493	642	321	321
NP_005424	NP_001387	736	368	368	540	270	270
NP_005424	NP_003984	736	368	368	166	83	83
NP_005424	NP_004705	736	368	368	164	82	82
NP_005424	NP_004062	736	368	368	176	88	88
AAC63054	AAF04852	446	223	223	1,364	682	682
AAC63054	NP_004337	446	223	223	1,558	779	779
AAC63054	AAA51985	402	201	201	182	91	91
AAC63054	AAI29989	446	223	223	1,594	797	797
AAC63054	AAH14460	438	219	219	130	65	65
AAF04852	NP_004337	654	327	327	718	359	359
AAF04852	AAI29989	682	341	341	696	348	348
NP_004337	AAI29989	804	402	402	758	379	379
AAA51985	AAI29989	210	105	105	1,598	799	799
AAA51985	AAH14460	194	97	97	118	59	59
NP_004358	NP_000901	116	58	58	176	88	88
NP_004358	EAW86722	116	58	58	700	350	350
NP_004358	NP_000900	116	58	58	208	104	104
NP_004358	AAH14970	116	58	58	244	122	122

Continued on next page

Table S2 – continued from previous page

target(P)	target(Q)	$ \mathcal{X}_{B_P} $	$ \mathcal{X}_{B_P}^+ $	$ \mathcal{X}_{B_P}^- $	$ \mathcal{X}_{B_Q} $	$ \mathcal{X}_{B_Q}^+ $	$ \mathcal{X}_{B_Q}^- $
NP_004358	BAB91222	116	58	58	182	91	91
NP_004358	NP_001516	116	58	58	312	156	156
NP_004221	EAW86722	138	69	69	700	350	350
NP_004221	NP_001516	138	69	69	312	156	156
NP_004221	NP_004942	138	69	69	138	69	69
NP_000901	EAW86722	174	87	87	700	350	350
NP_000901	BAB91222	176	88	88	182	91	91
NP_000901	NP_001516	176	88	88	312	156	156
EAW86722	AAH14970	700	350	350	250	125	125
EAW86722	BAB91222	700	350	350	182	91	91
EAW86722	NP_001516	700	350	350	312	156	156
NP_000900	BAB91222	208	104	104	182	91	91
NP_000900	NP_001516	208	104	104	312	156	156
NP_000900	NP_004942	208	104	104	138	69	69
AAH14970	BAB91222	252	126	126	182	91	91
AAH14970	NP_001516	252	126	126	310	155	155
AAH14970	NP_004942	252	126	126	138	69	69
NP_002721	NP_001387	142	71	71	540	270	270
NP_002721	NP_003984	142	71	71	166	83	83
NP_002721	NP_004705	142	71	71	164	82	82
NP_002721	NP_004062	142	71	71	176	88	88
BAB91222	NP_004942	182	91	91	138	69	69
NP_003605	NP_004942	362	181	181	138	69	69

Continued on next page

Table S2 – continued from previous page

target(P)	target(Q)	$ \mathcal{X}_{B_P} $	$ \mathcal{X}_{B_P}^+ $	$ \mathcal{X}_{B_P}^- $	$ \mathcal{X}_{B_Q} $	$ \mathcal{X}_{B_Q}^+ $	$ \mathcal{X}_{B_Q}^- $
NP_001387	EAW70217	488	244	244	260	130	130
EAW70217	NP_003984	278	139	139	136	68	68
EAW70217	NP_004705	280	140	140	132	66	66
EAW70217	NP_004062	280	140	140	142	71	71
NP_001124480	NP_002825	128	64	64	318	159	159

In this table, the first two columns target(P) and target(Q) correspond to the accession numbers of the two target proteins corresponding to the two bioassays P and Q of the pair, respectively. The columns $|\mathcal{X}_{B_A}|$, $|\mathcal{X}_{B_A}^+|$ and $|\mathcal{X}_{B_A}^-|$ correspond to the number of total compounds, active compounds and inactive compounds in the bioassay A where ($A = \{P, Q\}$ of each pair).

3 Supplementary Results

3.1 Hyperparameter Configurations

Table S3: Hyperparameter Configurations

parameter	values
α	0, 0.1, 0.5, 1, 2
λ	0.001, 0.01, 0.5, 1
dimension d	25, 50, 100
# message passing steps τ	2, 3, 4
hidden layer size in $f_a(\cdot)$	100
hidden layer size in L, G and S	100
batch size	10
learning rate	1e-3

Table S3 presents the hyperparameter configurations for all our methods. α and λ correspond to the trade-off parameter between the source and target classification losses as in

Equation 4) and the trade-off parameter between the classification and discriminator losses in Equation 13), respectively. α is only associated with TAc and TAc-fc; whereas λ is only associated with TAc-fc and its variants. We tried 3 different values for d which represents the dimension of the compound representation out of GNN and dmpna; and 3 different values for the number of message passing steps τ . Hence, these two hyperparameters are associated with all methods except FCN-morgan and FCN-morganc. The hidden layer size in the attention network denoted by $f_a(\cdot)$, the feature-wise discriminator denoted by L, and the compound-wise discriminator denoted by G is fixed to 100. We used a fixed batch size of 10 and an initial learning rate of 1e-3 with exponential decay every epoch from 1e-3 to 1e-4 at the end of training. We trained each model for 40 epochs with an early-stopping criteria based on the ROC-AUC performance on the validation set. Specifically, during training, we evaluated the ROC-AUC performance of each model on the validation set at every epoch; and we choose the trained model at some epoch k that gives the best performance on the validation set.

3.2 Prediction Analysis

Table S4 presents the pairwise similarity analysis for active compounds which were correctly classified by TAc-c, but incorrectly classified as inactive by TAc, TAc-fc and its variants.

Table S4: Similarity analysis of correct predictions by TAc-c

source(S)	target(T)	#cor	#act	cor%	$\text{sim}(\tilde{\mathcal{X}}_{B_T}^+, \mathcal{X}_{B_S}^+)$	$\text{sim}(\tilde{\mathcal{X}}_{B_T}^+, \mathcal{X}_{B_T}^+)$	sdiff%	e-sdiff%	p-value
EAW86722	AAI27629	36	128	28.125	0.231	0.194	19.401	21.692	1.68e-05
NP_004818	ABD72211	131	485	27.010	0.191	0.218	-12.557	-12.312	3.05e-20
NP_000901	NP_001516	33	124	26.613	0.213	0.182	17.135	19.886	2.57e-05
NP_000483	NP_000918	18	82	21.951	0.262	0.444	-41.090	-32.693	1.56e-05
NP_004942	NP_003605	29	145	20.000	0.164	0.174	-5.916	-2.832	4.15e-01
NP_004221	NP_001516	21	124	16.935	0.212	0.203	4.530	6.081	2.45e-01
AAC63054	AAF04852	85	546	15.568	0.255	0.249	2.490	3.969	1.25e-01

Continued on next page

Table S4 – continued from previous page

source(S)	target(T)	#cor	#act	cor%	sim($\tilde{\mathcal{X}}_{B_T}^+, \mathcal{X}_{B_S}^+$)	sim($\tilde{\mathcal{X}}_{B_T}^+, \mathcal{X}_{B_T}^+$)	sdiff%	e-sdiff%	p-value
NP_001516	NP_000947	15	112	13.393	0.244	0.193	26.449	28.965	2.92e-04
EAW86722	NP_004358	6	46	13.043	0.239	0.144	66.156	66.256	5.06e-06
AAH04460	AAH14460	6	55	10.909	0.228	0.154	47.925	50.102	2.68e-05
P00748	NP_004521	8	85	9.412	0.227	0.209	8.621	11.614	2.38e-01
P00748	AAF04852	50	546	9.158	0.237	0.267	-11.053	-8.667	1.22e-04
P00748	NP_660205	57	634	8.991	0.243	0.242	0.662	1.593	6.55e-01
NP_004942	NP_000676	15	168	8.929	0.183	0.216	-15.296	-11.831	8.28e-03
EAW86722	NP_000947	10	112	8.929	0.240	0.208	15.663	17.138	1.41e-01
AAC63054	AAI29989	55	638	8.621	0.234	0.249	-6.064	-3.701	1.69e-02
NP_001391	NP_001516	10	123	8.130	0.269	0.201	33.649	34.022	1.13e-06
EAW86722	AAH14970	8	99	8.081	0.266	0.212	25.838	28.634	1.58e-02
AAI29989	AAF04852	22	273	8.059	0.315	0.213	48.214	50.797	3.80e-10
NP_036559	AAI29989	51	636	8.019	0.244	0.258	-5.124	-4.478	5.37e-03
BAB91222	AAH14970	8	101	7.921	0.175	0.165	5.943	8.653	3.60e-01
P00748	NP_036559	5	67	7.463	0.271	0.184	47.440	43.716	8.58e-02
NP_004358	AAH14970	7	98	7.143	0.207	0.167	24.161	23.704	9.37e-03
AAA51985	NP_036559	5	70	7.143	0.226	0.167	35.308	35.516	1.30e-03
BAB91222	NP_000901	5	71	7.042	0.252	0.166	51.322	52.216	2.77e-02
NP_004358	NP_001516	8	124	6.452	0.195	0.196	-0.357	2.666	9.42e-01
AAH14460	AAC63054	11	176	6.250	0.240	0.237	1.395	4.762	8.31e-01
NP_003984	EAW70217	7	112	6.250	0.176	0.207	-15.381	-10.736	2.51e-01
NP_001516	NP_000676	10	168	5.952	0.215	0.177	21.813	25.027	4.71e-02
NP_000900	NP_001391	16	273	5.861	0.207	0.187	10.512	13.962	5.45e-02
EAW86722	NP_000901	4	70	5.714	0.211	0.153	37.288	39.267	3.66e-04
NP_004062	NP_005424	16	294	5.442	0.178	0.191	-6.695	-4.963	1.83e-01

Continued on next page

Table S4 – continued from previous page

source(S)	target(T)	#cor	#act	cor%	sim($\tilde{\mathcal{X}}_{B_T}^+, \mathcal{X}_{B_S}^+$)	sim($\tilde{\mathcal{X}}_{B_T}^+, \mathcal{X}_{B_T}^+$)	sdiff%	e-sdiff%	p-value
NP_001516	AAB26273	12	222	5.405	0.192	0.173	11.478	13.326	2.22e-02
AAH14460	P00748	6	118	5.085	0.209	0.176	19.259	19.193	9.09e-03
ADZ17337	NP_000448	6	119	5.042	0.216	0.378	-42.872	-26.487	7.48e-02
EAW86722	AAB26273	11	222	4.955	0.171	0.172	-0.639	-0.201	9.25e-01
AAB26273	AAH14970	5	101	4.950	0.237	0.191	23.628	30.287	1.59e-01
AAI28575	ADZ17337	3	62	4.839	0.195	0.122	59.508	59.696	6.99e-03
NP_004358	AAB26273	10	222	4.505	0.180	0.181	-0.222	1.167	9.65e-01
P00748	NP_004337	27	623	4.334	0.244	0.271	-9.934	-7.917	2.86e-03
AAB26273	NP_000901	3	70	4.286	0.200	0.158	26.692	33.966	1.20e-01
AAB26273	NP_000676	7	167	4.192	0.217	0.294	-26.226	-17.244	1.02e-01
AAA51985	P00748	4	98	4.082	0.254	0.185	37.324	38.576	3.26e-02
AAA51985	AAI29989	26	639	4.069	0.227	0.243	-6.579	-5.651	1.71e-02
AAB26273	EAW86722	11	280	3.929	0.253	0.359	-29.579	-7.283	1.26e-01
NP_036559	AAF04852	21	545	3.853	0.224	0.237	-5.495	-3.310	2.10e-01
AAH14460	AAH04460	13	356	3.652	0.154	0.136	12.702	12.870	1.06e-04
NP_004358	NP_000900	3	83	3.614	0.211	0.181	16.860	15.934	1.37e-01
NP_000901	EAW86722	10	280	3.571	0.251	0.503	-50.099	-46.770	1.25e-04
NP_004818	NP_000483	5	143	3.497	0.205	0.190	8.065	8.009	1.57e-01
AAF04852	AAC63054	6	179	3.352	0.318	0.215	48.069	49.310	5.66e-04
AAI29989	NP_660205	12	395	3.038	0.287	0.191	49.869	52.166	3.98e-05
NP_775180	ADZ17337	2	67	2.985	0.181	0.143	26.606	25.601	2.58e-01
NP_000448	ADZ17337	2	68	2.941	0.114	0.060	91.779	95.379	7.93e-02
ADZ17337	NP_066285	4	137	2.920	0.221	0.204	8.640	10.717	2.39e-01
AAC63054	NP_004337	18	623	2.889	0.264	0.271	-2.731	0.234	5.85e-01
NP_004358	NP_000901	2	71	2.817	0.154	0.123	25.345	26.218	3.06e-01

Continued on next page

Table S4 – continued from previous page

source(S)	target(T)	#cor	#act	cor%	sim($\tilde{\mathcal{X}}_{B_T}^+, \mathcal{X}_{B_S}^+$)	sim($\tilde{\mathcal{X}}_{B_T}^+, \mathcal{X}_{B_T}^+$)	sdiff%	e-sdiff%	p-value
AAF04852	NP_004337	8	287	2.787	0.321	0.218	47.407	50.401	6.15e-03
AAB26273	NP_000947	3	108	2.778	0.232	0.158	46.717	52.124	7.21e-02
AAB26273	NP_003605	4	144	2.778	0.219	0.151	44.746	43.328	3.17e-02
NP_000901	BAB91222	2	73	2.740	0.266	0.584	-54.493	-54.476	2.78e-02
AAH14970	AAB26273	6	222	2.703	0.191	0.164	16.190	16.216	7.96e-02
BAB91222	AAB26273	6	222	2.703	0.160	0.167	-4.540	-3.455	2.74e-01
BAB91222	NP_000947	3	112	2.679	0.206	0.214	-3.745	-2.894	7.53e-01
P00748	AAC63054	4	153	2.614	0.259	0.249	3.974	5.017	7.69e-01
BAB91222	NP_001391	7	276	2.536	0.158	0.183	-13.803	-13.149	1.29e-02
AAH14460	NP_036559	2	81	2.469	0.246	0.186	32.453	32.468	6.44e-02
NP_004337	P00748	3	128	2.344	0.270	0.191	41.575	43.957	1.01e-02
AAI29989	NP_036559	2	87	2.299	0.227	0.150	52.107	51.804	3.36e-01
NP_004337	AAC63054	4	179	2.235	0.283	0.197	43.357	42.784	4.74e-03
NP_000760	NP_000752	17	828	2.053	0.265	0.197	34.518	40.100	4.00e-05
AAA51985	AAC63054	3	160	1.875	0.263	0.212	24.034	24.481	8.67e-03
NP_000903	EAW86722	5	267	1.873	0.236	0.507	-53.336	-52.539	1.96e-03
NP_000900	AAB26273	4	222	1.802	0.192	0.172	11.874	21.471	5.88e-01
NP_612200	AAB26273	4	222	1.802	0.205	0.192	7.035	12.079	6.27e-01
NP_004705	EAW70217	2	112	1.786	0.176	0.153	15.465	15.582	3.20e-03
AAI29989	AAC63054	3	179	1.676	0.275	0.195	40.963	43.788	1.15e-01
EAW86722	NP_000903	2	121	1.653	0.201	0.119	68.483	73.823	1.13e-02
BAH02301	AAI28575	4	243	1.646	0.199	0.155	28.479	30.254	2.86e-02
AAI29989	P00748	2	128	1.563	0.307	0.187	63.821	68.477	2.76e-01
NP_660205	P00748	2	128	1.563	0.223	0.199	12.042	18.287	3.47e-01
NP_000762	NP_000752	11	768	1.432	0.252	0.223	12.713	16.400	7.20e-02

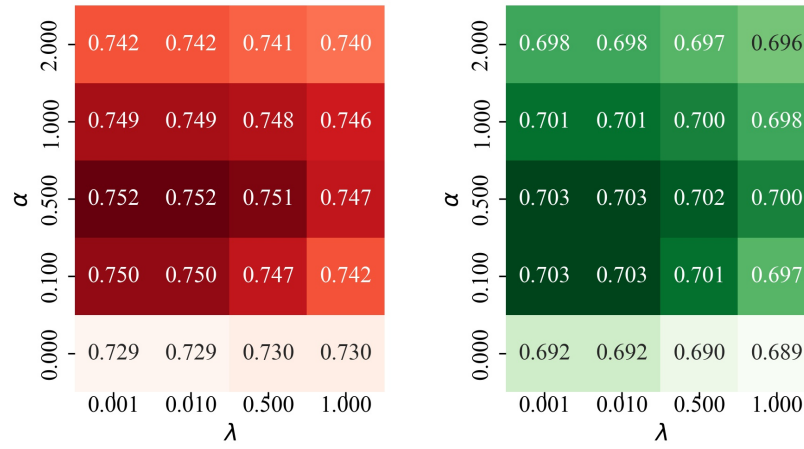
Continued on next page

Table S4 – continued from previous page

source(S)	target(T)	#cor	#act	cor%	$\text{sim}(\tilde{\mathcal{X}}_{B_T}^+, \mathcal{X}_{B_S}^+)$	$\text{sim}(\tilde{\mathcal{X}}_{B_T}^+, \mathcal{X}_{B_T}^+)$	sdiff%	e-sdiff%	p-value
BAB91222	EAW86722	4	280	1.429	0.212	0.395	-46.403	-45.265	1.19e-02
NP_000918	NP_000483	2	143	1.399	0.181	0.167	8.313	8.153	2.06e-01
NP_066285	AAI28575	3	244	1.230	0.224	0.175	28.138	28.295	3.79e-02
P00748	AAI29989	7	638	1.097	0.234	0.325	-27.930	-17.446	1.11e-01
AAB26273	NP_001391	3	274	1.095	0.236	0.220	7.039	8.095	7.11e-01
NP_004942	NP_997055	19	2,020	0.941	0.174	0.233	-25.354	-24.636	1.43e-07
NP_002721	NP_001387	2	216	0.926	0.157	0.262	-40.099	-15.747	5.69e-01
NP_001387	NP_065717	3	411	0.730	0.303	0.358	-15.284	-11.201	3.77e-01
AAF04852	AAI29989	2	278	0.719	0.233	0.190	22.866	23.111	5.88e-02
NP_000947	EAW86722	2	280	0.714	0.219	0.166	31.671	31.738	6.30e-04
NP_004337	AAI29989	2	303	0.660	0.272	0.211	28.856	28.826	6.91e-02
NP_004705	NP_005021	50	8,158	0.613	0.163	0.249	-34.671	-33.500	5.32e-14
NP_000752	NP_000760	3	543	0.552	0.299	0.247	21.330	23.816	3.93e-01
NP_036559	NP_004337	2	622	0.322	0.252	0.246	2.153	3.971	8.75e-01
NP_002825	NP_004081	2	1,316	0.152	0.261	0.254	2.678	2.762	8.02e-03

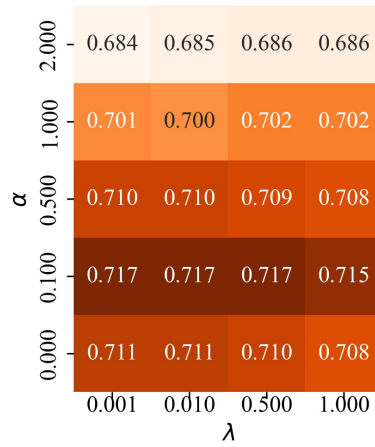
In this table, the columns source(S) and target(T) correspond to the protein accession numbers of the corresponding bioassays of source and target tasks, respectively. The columns #cor, #act and cor% have the count of correctly classified active compounds, total number of active compounds and the percentage of correctly classified active compounds, respectively. Such compounds are denoted by the set $\tilde{\mathcal{X}}_{B_T}^+$. The columns $\text{sim}(\tilde{\mathcal{X}}_{B_T}^+, \mathcal{X}_{B_S}^+)$ and $\text{sim}(\tilde{\mathcal{X}}_{B_T}^+, \mathcal{X}_{B_T}^+)$ present the average pairwise similarities of correctly classified compounds in $\tilde{\mathcal{X}}_{B_T}^+$ with their top-5 most similar active compounds from the source and target bioassay, respectively. The column sdiff% has the percentage difference of the average pairwise similarities from the source compounds over the target compounds. The column e-sdiff% has the average of element-wise percentage difference of similarities from the source active compounds over the target active compounds. The column p-value has the corresponding p-values for e-sdiff%.

3.3 Parameter Study: TAc-fc-dmpna

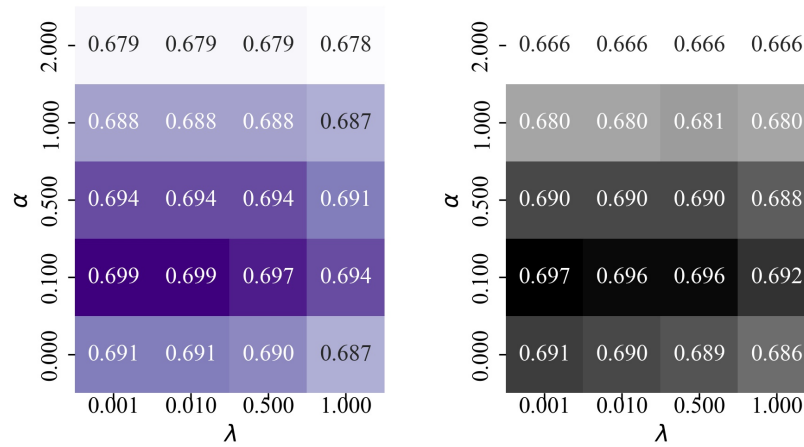


(a) PR-AUC

(b) precision



(c) sens



(d) accuracy

(e) F1 score

Figure S1: Parameter Study of TAc-fc-dmpna

Figure S1 presents the parameter study in TAc-fc-dmpna in terms of PR-AUC, precision, sens, accuracy and F1 on α (i.e., the trade-off parameter between the source and target classification losses as in Equation 4) and λ (i.e., the trade-off parameter between the classification and discriminator losses in Equation 13). The study was conducted over the tasks for which TAc-dmpna outperforms the other methods in respective metrics. The values in each cell in the figure represent the average of the best performance over the tasks with the optimal choice of other hyperparameters.

Figure S1 shows that TAc-fc-dmpna has the best performance in PR-AUC when $\alpha = 0.5$ and $\lambda = 0.001$ and 0.01 . This aligns with our observations in the parameter study for ROC-AUC. TAc-fc-dmpna has the best performance in precision, sens, accuracy and F1 when $\alpha = 0.1$ and $\lambda = 0.001$ and 0.01 . Although for the metrics except ROC-AUC and PR-AUC, the best performance is achieved at a lower α than 0.5 , optimal α values are still non-zero. This provides strong evidence that the target task benefits from the transferred information from the source task. Similar to our observed trends from the parameter study for ROC-AUC, there is a significant performance drop for too high or too low α , regardless of what λ is; for optimal α , a $\lambda = 0.001$ or 0.01 gives the best performance; for a given α , higher λ values degrades the performance.

4 Compound Prioritization using dmpna

In this section, we develop a comprehensive learning-to-rank method for effective compound prioritization that jointly learns molecular graph representations via GNN and a scoring function $\phi(\cdot)$ using the representations in an end-to-end manner. We denote our method as **gnnCP**. We consider the compound prioritization problem to correctly rank compounds in terms of their activities with respect to a protein target. To achieve so, **gnnCP** represents compounds using latent features that are learned from molecular graphs via a new, attention directed message passing neural network (**dmpna**) (explained in Section 4.2.2). We use

a linear scoring function $\phi(\mathbf{r}_c) : \mathbb{R}^d \rightarrow \mathbb{R}$ to score the compounds as follows,

$$\phi(\mathbf{r}_c) = \mathbf{w}^\top \mathbf{r}_c, \tag{7}$$

where \mathbf{w} is a learnable parameter. Our proposed method **gnnCP** will produce a ranking of compounds induced by their predicted scores (computed using $\phi(\mathbf{r}_c)$). Compounds with higher predicted scores will be ranked higher than those with lower predicted scores. Higher scores will be assigned to more active compounds in order to achieve the best ranking quality. To quantify the ranking quality, we use the popular metric non-concordance index (*nCI*). *nCI* measures the fraction of incorrectly ranked compound pairs as follows,

$$nCI(r, \phi) = \frac{1}{|\{c_i, c_j | c_i \succ_r c_j\}|} \sum_{\{c_i, c_j | c_i \succ_r c_j\}} \mathbb{I}(c_i \preceq_\phi c_j), \tag{8}$$

where \mathbb{I} is the indicator function. In equation 8, $c_i \succ_r c_j$ represents a pair of compounds c_i and c_j such that c_i is ranked higher than c_j in the ground truth ranking r , and $c_i \preceq_\phi c_j$ represents that c_i is ranked lower than c_j in the predicted ranking structure induced by ϕ . In essence, a lower *nCI* would indicate better ranking performance. Following the work,¹ we use *nCI* over the predicted ranking structure induced by ϕ as our loss function \mathcal{L}_{rank} .

Since the indicator function in equation 8 is discontinuous, we use the logistic loss as a surrogate function² as follows,

$$\mathbb{I}(a \preceq b) \approx \log(1 + \exp(-(a - b))). \tag{9}$$

The loss term \mathcal{L}_{rank} for the set of compounds in a given bioassay is defined as follows,

$$\mathcal{L}_{rank} = \frac{1}{|\{c_i, c_j | c_i \succ_r c_j\}|} \sum_{\{c_i, c_j | c_i \succ_r c_j, c_i \preceq_\phi c_j\}} \log[1 + \exp(-(\mathbf{w}^\top \mathbf{z}_{c_i} - \mathbf{w}^\top \mathbf{z}_{c_j}))]. \tag{10}$$

We solve the following optimization:

$$\min_{\Theta} \mathcal{L}_{rank} + \lambda \|\Theta\|_2^2, \quad (11)$$

where λ is the regularization parameter and Θ is the set of trainable parameters. The above optimization encourages correct ranking of compound pairs and hence, higher scores being assigned to more active compounds.

References

- (1) Liu, J.; Ning, X. Differential compound prioritization via bidirectional selectivity push with power. *J. Chem. Inf. Model.* **2017**, *57*, 2958–2975.
- (2) Li, H. A short introduction to learning to rank. *IEICE Trans. Inf. Syst.* **2011**, *E94-D*, 1854–1862.